

4 Neutrino Measurements (WBS 1.3.4)

Introduction



The main goal of the LBNE Near Detectors (ND) is to measure the background neutrino interaction event rate from water and argon targets, before neutrino oscillations have occurred, and to extrapolate this background rate to the far detectors. Both water and argon targets are needed because the two far detector technologies being considered are: (i) a 100-kT water Cherenkov detector; (ii) a 20-kT liquid argon (LAr) TPC. In addition, due to the somewhat different neutrino fluxes at the near and far locations, it will also be important with the ND to measure the ν_μ , $\bar{\nu}_\mu$, ν_e and $\bar{\nu}_e$ fluxes and to measure the cross sections of the various contributions to the background. The extrapolation of the neutrino fluxes from the near to the far locations will be dependent on the neutrino energy, so that the extrapolation of the charged-current intrinsic ν_e background will be different, for example, from the extrapolation of the neutral-current π^0 background. The main focus will be in the energy range $E_\nu < 5$ GeV, although higher neutrino energies are also of interest.

Other physics goals of the ND will include searches/measurements for high Δm^2 neutrino oscillations and sterile neutrino decay, the measurement of $\sin^2\theta_{\text{ws}}$, the determination of $\Delta(s)$, and measuring the A dependence of the charged-current quasi-elastic neutrino cross section. These additional goals will not only broaden the physics reach of LBNE, but may also, as in the case of high Δm^2 neutrino oscillations, prove critical to the measurement of neutrino oscillations in the far detector.

Event Rates

All of the event rates were generated using the LBNE 2008 NuMI-based reference fluxes [1]. Assuming these fluxes, the v3 NUANCE event generator [2] was used to simulate neutrino interaction cross sections, nuclear effects, and final state interactions. For simplicity, all event rates were generated assuming a water target and are provided per ton of water for 1E20 POT. (Note that the nominal rate of protons is 7.3E20 POT/year.) The proton energy is assumed to be 120 GeV, the horn current is 250 kA, and the decay pipe has a radius of 2 m and a length of 280 m. The distance from the target to the entrance of the near-detector hall is 670 m.

These rates were evaluated assuming a flux distribution generated at the center of the near detector and were not given any radial-dependence across the face of the detector. Given present flux and cross section uncertainties, these event rate estimates are accurate to $\sim 20 - 50\%$.

Table 1 lists the resultant event yields in the LBNE near detector at 670m for a 120 GeV beam. Note that the total ν_μ event rate (flux times cross section) at 670m is a factor of ~ 2.6 larger than previously presented rates that were calculated at 1km [3, 5]).

Production Mode	Number of ν_μ events
CC QE ($\nu_\mu n \rightarrow \mu^- p$)	18,977
NC elastic ($\nu_\mu N \rightarrow \nu_\mu N$)	7,094
CC resonant π^+ ($\nu_\mu N \rightarrow \mu^- N \pi^+$)	25,821
CC resonant π^0 ($\nu_\mu n \rightarrow \mu^- p \pi^0$)	6,308
NC resonant π^0 ($\nu_\mu N \rightarrow \nu_\mu N \pi^0$)	6,261
NC resonant π^+ ($\nu_\mu p \rightarrow \nu_\mu n \pi^+$)	2,694
NC resonant π^- ($\nu_\mu n \rightarrow \nu_\mu p \pi^-$)	2,325
CC DIS ($\nu_\mu N \rightarrow \mu^- X, W > 2$)	29,989
NC DIS ($\nu_\mu N \rightarrow \nu_\mu X, W > 2$)	10,183
NC coherent π^0 ($\nu_\mu A \rightarrow \nu_\mu A \pi^0$)	790
CC coherent π^+ ($\nu_\mu A \rightarrow \mu^- A \pi^+$)	1,505
NC resonant radiative decay ($N^* \rightarrow N \gamma$)	41
$\nu_\mu e^- \rightarrow \nu_\mu e^-$	11
IMD ($\nu_\mu e \rightarrow \mu^- \nu_e$)	6
Other	17,023
Total CC	94,948
Total NC+CC	129,028



Table 4-1: Estimated ν_μ rates in neutrino mode per ton water

Estimated ν_μ rates in neutrino mode per ton water for 1×10^{20} POT at 670m assuming a 120 GeV proton beam, 250kA horn current, and a 2-m radius 280-m long decay region [1]. Processes are defined at the initial neutrino interaction vertex and thus do not include final state effects. These estimates do not include detector efficiencies or acceptance.

The anti- ν_μ flux in antineutrino mode is similar to the ν_μ flux in neutrino mode. There is a sizable contamination of neutrinos in the antineutrino beam; hence both contributions are listed in the corresponding event rate table (Table 2). After cross section weighting, the beam is almost a 50/50 mix of neutrinos and antineutrinos: anti- ν_μ (ν_μ) interactions comprise 57% (43%) of the total antineutrino mode muon-flavor event rate.

Comparing Tables 1 and 2, the total anti- $\nu_\mu + \nu_\mu$ rate in antineutrino mode is estimated to be about 66% of the total ν_μ rate in neutrino mode, so the overall event yields are somewhat smaller in antineutrino running.

Production Mode	Number of anti- ν_μ events	Number ν_μ events
CC QE	11,097	2,185
NC elastic	3,789	847
CC resonant π^+	0	3,569
CC resonant π^-	8,762	0
CC resonant π^0	2,829	933
NC resonant π^0	3,008	877
NC resonant π^+	1,352	414
NC resonant π^-	1,086	364
CC DIS	5,685	17,645
NC DIS	2,345	5,625
NC coherent π^0	644	132
CC coherent π^+	0	259
CC coherent π^-	1,224	0
NC resonant radiative decay	21	5
$\nu_\mu e^- \rightarrow \nu_\mu e^-$	7	3
IMD ($\nu_\mu e^- \rightarrow \mu^- \nu_e$)	0	5
Other	6,668	3,476
Total CC	34,319	27,065
Total NC+CC	48,517	36,339

Table 4-2: Estimated anti ν_μ and ν_μ rates in antineutrino mode per ton water

Estimated anti- ν_μ and ν_μ rates in antineutrino mode per ton water for 1×10^{20} POT at 670m assuming a 120 GeV proton beam, 250kA horn current, and a 2m radius 280m long decay region [1]. Processes are defined at the initial neutrino interaction vertex and thus do not include final state effects. These estimates do not include detector efficiencies or acceptance. In almost all cases, the ν_μ rates are about 20–30% of the corresponding anti- ν_μ rates with the exception of the DIS channels, where the ν_μ rates are roughly 2-3 times larger than that for anti- ν_μ 's. This is due to the larger high energy flux tail for ν_μ 's relative to anti- ν_μ 's.

4.1 Requirements and Specifications

A. Different Detector Module Design Options

There are two options for the ND reference design. The first option (the Scintillator Tracker Option) includes a H2/D2 target, followed by a LAr TPC (MicroBooNE or UCLA LAr), followed by the MINERvA detector, followed by a fraction (~25%) of MINOS. The second option (the Straw Tube Tracker Option) includes a H2/D2 target, followed by a LAr TPC (MicroBooNE or UCLA LAr), followed by HiResMnu. Not accounting for spacing, the total length of both options is

~90 ft, so that we will need the full ~112-ft length of the Reference ND Hall Design. The floor and ceiling should be horizontal (flat) as shown in the Reference ND Hall Design. The floor to ceiling height of 45 ft, with a 35-ft +/- clear height to the crane hook is sufficient. The nominal size of the surface building is 50 ft × 125 ft × 35 ft.

For the H₂/D₂ target, we initially thought of building a bubble chamber. However, as that may not be feasible, we are now considering running with targets of H₂O and D₂O interspersed in either the Scintillator or Straw Tube tracker.

The LAr detector will have several requirements: (i) low humidity to prevent icing and water absorption in the insulation; (ii) fairly stable temperature control (20±2C); (iii) an ODH area for the cryostat and an over-pressured non-ODH area with air-tight doors for the electronics; (iii) "beefy" ventilation systems in both areas; (iv) cables with flame-resistant insulation/covering. The total amount of liquid argon is in the range from 100-350 tons.

The total power requirement for the Scintillator Tracker option is ~125kW. From experience with MINOS, it was requested that there be a Drip Ceiling to route ground-water seepage away from the detector.

The total power requirement for the Straw Tube Tracker option is ~2MW. In addition, the magnet for HiResMnu detector has a weight of ~1000 tons and requires a water flow of ~2000 l/m. The gas volume for the straw tubes includes ~100K cc of N₂ and ~33K cc of Xe/CO₂.

B. Fiducial Volume & Geometry Requirements



The reference Fiducial Volumes for the detectors are the following: 50m³ (70 tons) for the LAr detector and 50m³ (5 tons) for the Fine-Grained detector. For the LAr detector, the nominal wire pitch, electron drift attenuation length, and Ar purity are 3mm, 5m, and 100 ppt, respectively.

C. Vertex Resolutions

The detector vertex resolutions must be sufficiently good to separate electrons from gammas and to observe the recoil protons from the event vertex. Averaged over the fiducial volume, the reference vertex resolutions are the following: <1cm for the LAr detector and <1cm for the Fine-Grained detector.

D. Angular Resolutions

Excellent angular resolution is needed to measure the angular distribution of neutrino events and to reconstruct the incident neutrino angular distribution. In addition, excellent angular resolution is necessary for measuring neutrino-electron elastic scattering events. Averaged over the fiducial volume, the reference angular resolution for electrons and muons is 10 mrad.

E. Energy Resolutions

Good energy resolution is needed to reconstruct the energy of the incident neutrinos. Averaged over the fiducial volume, the reference energy resolution for electrons and muons is 3-5%.

F. NC π^0 Rejection & Identification Efficiencies

NC π^0 events constitute one of the largest backgrounds in the search for ν_e and $\bar{\nu}_e$ appearance. The reference NC π^0 rejection & identification efficiencies are 95% and 50%, respectively, versus reconstructed neutrino energy.

G. NC gamma Rejection & Identification Efficiencies

NC gamma events are another large background in the search for ν_e and $\bar{\nu}_e$ appearance. The reference NC gamma rejection & identification efficiencies are 90% and 50%, respectively, versus reconstructed neutrino energy.

H. External Event Rejection & Identification Efficiencies

Neutrinos that interact outside the detector can produce gammas or neutrons that convert inside the fiducial volume of the detector. These events can be measured and rejected with veto detectors and by making use of reconstructed angular and position information. The reference external event rejection and identification efficiencies are 50-99% (depending on the event selection) and 50%, respectively.

I. CCQE ν_μ Rejection & Identification Efficiencies

The CCQE ν_μ event sample will be used to measure the ν_μ flux in the beam and the corresponding cross sections. The reference CCQE ν_μ rejection and identification efficiencies are 99% and 50%, respectively.

J. CCQE ν_e Rejection & Identification Efficiencies

The CCQE ν_e event sample will be used to measure the ν_e flux in the beam and the corresponding cross sections and to search for ν_e appearance in the far detector. The reference CCQE ν_e rejection and identification efficiencies are 90-99% and 50%, respectively.

K. Total Background vs Energy for CCQE ν_μ Selection

The CCQE ν_μ event sample will be used to measure the ν_μ flux in the beam and the corresponding cross sections. For the CCQE ν_μ selection, the reference total background is 25%.

L. Total Background vs Energy for CCQE ν_e Selection

The CCQE ν_e event sample will be used to measure the ν_e flux in the beam and the corresponding cross sections and to search for ν_e appearance in the far detector. For the CCQE ν_e selection, the reference total background is 50%.

M. Uncertainty of ν_μ , $\bar{\nu}_\mu$, ν_e and $\bar{\nu}_e$ Determination vs Energy

The reference uncertainty in the ν_μ and $\bar{\nu}_\mu$ determination is 5% for each. A magnetic field or magnetized steel will be needed to separate ν_μ from $\bar{\nu}_\mu$. The reference uncertainty in the ν_e and $\bar{\nu}_e$ determination is 5% for each. A magnetic field will be needed to separate ν_e from $\bar{\nu}_e$.

4.2 Neutrino Flux Measurement (WBS 1.3.4.2)

A. Neutrino Flux Detector (Overview)

To date, accelerator neutrino fluxes for neutrino energies between 0.3 to 3.0 GeV are poorly known. The uncertainty in neutrino flux is reflected in the uncertainty in neutrino cross sections, as displayed in Fig 1., where the $\nu_\mu + n \rightarrow \mu^- + p$ and $\bar{\nu}_\mu + p \rightarrow \mu^- + n$ cross sections are shown. It is evident that the knowledge of these important quantities is very poorly known for neutrinos and the situation is even worse for anti-neutrinos. In an experiment such as LBNE, it is necessary to know the flux at the near detector and to establish the changes in this flux at the far detector. Even in the absence of neutrino oscillations the flux at the near and far detectors will differ. This difference will have to come from MC simulation of the beam. Having a knowledge of the CCQE cross section of the nuclear constituents of the far detector as a function of ν energy is essential to correctly infer the neutrino flux at the far detector.

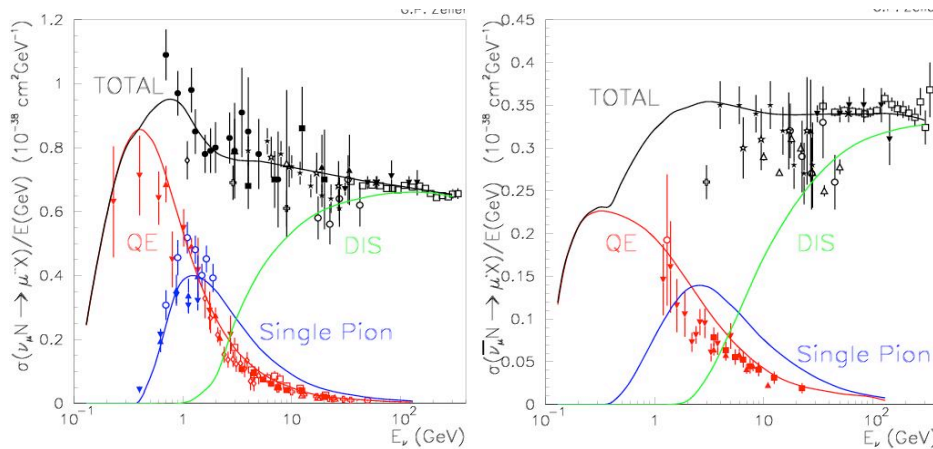


Figure 4-1. Neutrino and anti neutrino charged current cross sections $\sigma_{\nu/\bar{\nu}N} \rightarrow \mu^- X$ by the incident neutrino energy and the $A=N+Z$ in the material of the detector. The figure on the left is taken from [1,Ahn 2006] while the figure on the right is from xxx.

Specifying a neutrino flux $F_{\nu_i}(E_{\nu_i}, L)$ requires specifying the number of neutrinos of a particular energy and flavor, per unit area, per number of protons incident on the production target. Due to the presence of neutrino oscillations, this flux will also be a function of distance (L) from the neutrino's point of origin. The number of protons striking the target can be well measured (2%). The neutrinos originate from the decay of mesons in flight (mostly π and κ) produced in the collision of the accelerator beam with the production target. The mesons typically pass through a magnetic horn that focuses the momentum of sign selected mesons to intercept the detector. This magnetic focusing increases the flux of neutrinos at the detector by factors of 4 to 7. While

calculation of the neutrino flux via Monte Carlo simulation would seem straight forward, its dependence on detailed input information (pion momentum distributions, secondary interactions in target, condition of the target etc) makes the calculation useful for design purposes, but not reliable as an absolute flux prediction to better than 30%. In a case [2,] where considerable time and effort was expended making the necessary measurements to constrain the calculated prediction at the 10% level, surprising results on resulting cross sections emerged [3,]. At present it would be difficult to be certain that any neutrino-nucleus cross section or neutrino flux is known to better than 20%.

The flux uncertainty is directly tied to the fact that there is no readily accessible neutrino-nucleus cross section that can be calculated with the requisite certainty. The uncertainty in what is termed charged current quasi elastic (CCQE) scattering is at best 20%, even though such cross sections have often been used to determine the flux. The figure below represents the conventional picture of a CCQE reaction.

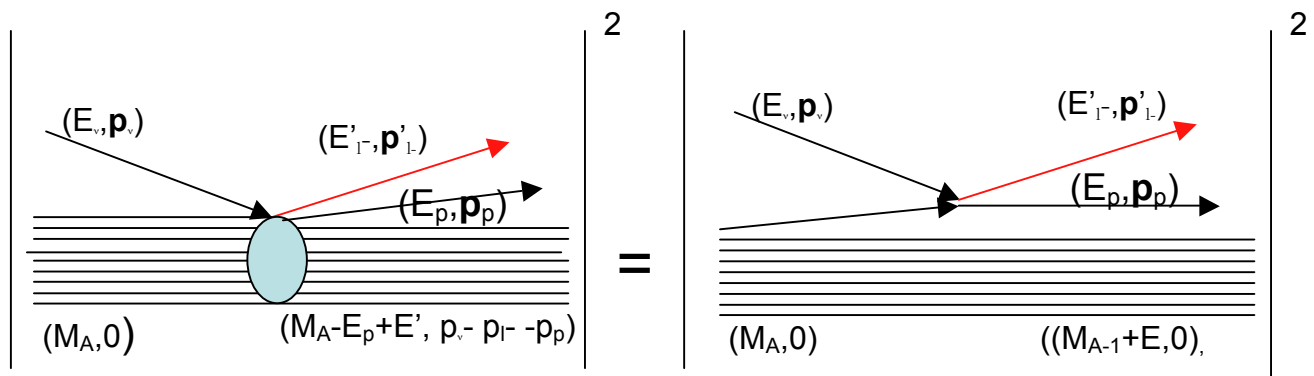
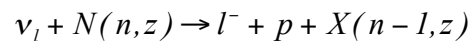


Figure 4-2 The cartoon to the right illustrates the simple approximation to CCQE ν scattering on a nuclear target. The underlying complexity of the nuclear matter is approximated as a Fermi Gas in which the individual nucleons move independently with a simplified momentum distribution. In cases where only the energy and momentum of the outgoing charged lepton are measured, there is much uncertainty in establishing the incident neutrino energy, E_ν .

Figure 2 shows a neutrino interaction with a nucleus, where energy $E_\nu - E'_l$ and momentum $\mathbf{p}_\nu - \mathbf{p}'_l$ is transferred without the appearance of a meson in the final state and is approximated by a collision with a single nucleon in the nucleus. Furthermore, that nucleon is treated as an independent particle with a negative energy and initial momentum \mathbf{p}_n . Given the complexity of nuclear effects, the representation on the right hand side of the above figure is a cartoon of what actually occurs in a “quasi-elastic collision “. The calculation suggested by the right hand side is a useful benchmark to compare to experimental results but hardly a basis for a quantitative calculation of the expected cross section.

In many detectors (e.g. Cherenkov water detectors), all that is observed is the momentum of the outgoing charged lepton. The neutrino beam has a very large spread in incident energy and because the nucleons in a nucleus have an initial Fermi momentum, the incident neutrino energy cannot be determined to much better than 10%. Even this determination depends on using simple models of the nucleon’s momentum distribution and neglects the effects of short-range correlations, which further smear the determination of E_ν .

- [1] (K2K): M.H Ahn, et al, Phys. Rev. D74, 072003 (2006)
 [2] MiniBooNE Collaboration: A. A. Aguilar-Arevalo et al, Phys. Rev. D79, 072002 (2009)
 [3] MiniBooNE Collaboration: A. A. Aguilar-Arevalo et al, arXiv:1002.2680 hep-ex

B. The ideal neutrino flux detector (LD, LH bubble chamber)

The only way around the effects of E_ν smearing due to the uncertain initial nucleon momentum in a nucleus is to use hydrogen or deuterium targets. In the case of hydrogen, the nucleon is initially at rest and the two body kinematics of the reaction allows determination of E_ν limited only by the measurement of the charged lepton energy and angle. With deuterium the CCQE reaction is $\nu + d \rightarrow l^- + 2p$; the $2p$ final state allows direct measurement of the transferred energy and momentum, so that knowledge of E_ν is only limited by the measurement of the charged lepton energy ($\sim 3\%$) and may be assigned event by event. This is a unique feature of CCQE on deuterium

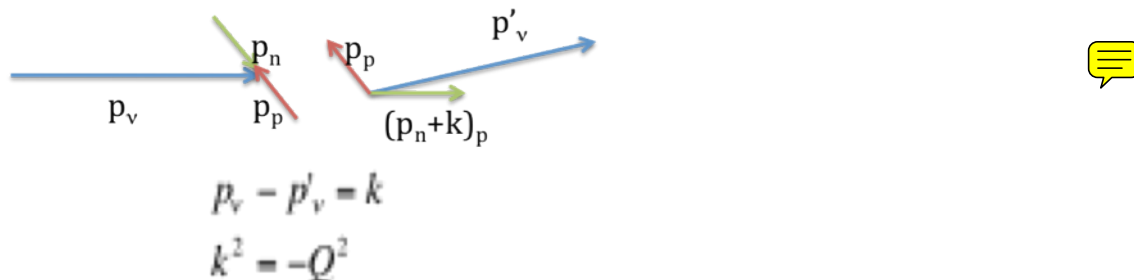


Figure 4-3: Diagram of unique property of CCQE scattering on deuterium

The 2 proton final state allows a direct assignment of the transferred energy and momentum. The vector quantities are all 4-vectors.

The use of deuterium and hydrogen targets not only overcomes the difficulty of establishing the neutrino energy, they are also the targets where the neutrino CCQE cross section can be most reliably calculated. In the case of hydrogen, there are no nuclear effects and the CCQE form factors [1] are well enough known that the quasielastic scattering for $Q^2 < 1$ (GeV/c)² is known to a few percent. In the case of deuterium, the two proton final state allows selecting values of the transferred momentum and energy where the calculated cross section is most certain. The ideal setup to access the $2p$ final state would be a bubble chamber with approximately 1 ton of liquid deuterium or 1/2 ton of hydrogen in a strong (~ 2 Tesla) magnetic field. The BNL 7 ft bubble chamber [2] is an example of just such a detector. Constructing such a device to present day safety standards would probably cost in excess of \$100M. Additionally, the LBNE ND will be some 400 ft underground with at least 2 other detectors in the same vault as the bubble chamber. Thus it appears that the bubble chamber option is not a suitable component of the ND complement.

- [1] H. Budd, A. Bodek, J. Arrington, Nuc Phys. B –Proceedings Supplements 139, 90 (2004)
 [2] J.A. Bamberger et al, NIM 130 378 (1975)

C. Workable compromises for LBNE ND

One option would be to incorporate LH and LD targets into a low-density fine grained detector, such a straw tube tracker. At the moment it is not seen how to accomplish this without incorporating unwanted mass to insulate LH or LD (20^0K) from the active elements of the tracker. A less desirable but more readily implemented solution is to use D_2O and H_2O . For CCQE ν interactions, a subtraction of H_2O from D_2O produces a yield due to neutrino scattering off the neutrons in deuterium. This subtraction would be carried out in bins of E_T and θ_T . With 1.25 tons of D_2O and 1.125 tons of H_2O , there should be $\sim 35,000$ CCQE events from deuterium per calendar year. Direct subtraction of the approximately four times greater O events from the H_2O target increases statistical uncertainty of the remaining deuterium sample by a factor of by a factor of 3. There is also a loss of information on the incident neutrino energy.

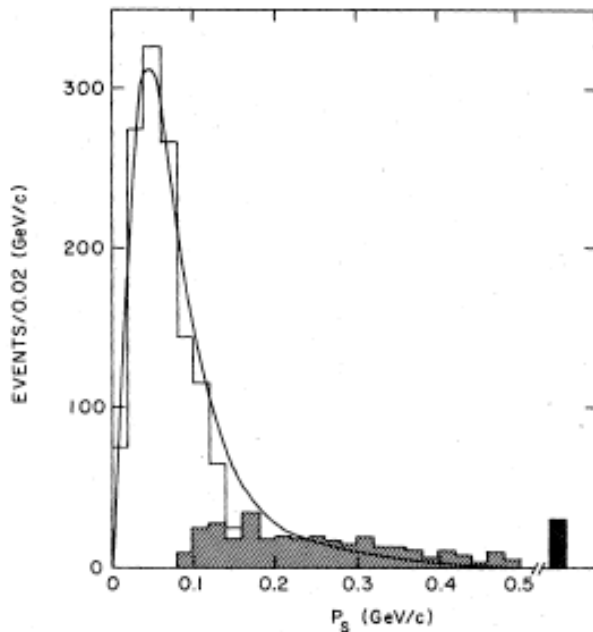


Figure 4-4: Momentum spectrum of the spectator proton in QE neutrino scattering off of deuterium [1]. The smooth curve is the prediction for the Hulthen wave function [2].

Because of its small binding energy, the Fermi momentum in deuterium, $0.06 \text{ GeV}/c$, is appreciably smaller than that in O, $0.235 \text{ GeV}/c$. Fig 1 above shows the momentum distribution of the spectator proton [1] in $\nu_\mu + d \rightarrow \mu^- + p + p_s$. The spectator proton is the proton initially in the deuteron. Its momentum is equal and opposite to the momentum of the charge-exchanged neutron in the CCQE reaction in the deuteron. The peak at $p_s \sim .05 \text{ GeV}/c$ corresponds to T_s of only 1.3 MeV. The spectator protons with higher momentum ($p_s > 0.25 \text{ GeV}/c$) were presumably involved in a short range correlation with the neutron when the CCQE event occurred. The momentum of the recoil proton from the CCQE reaction is the vector sum of transferred momentum (\vec{k}) plus its initial state Fermi momentum. Thus the transverse momentum of the emergent proton from deuterium should be more strongly correlated to that of the charged lepton than for a reaction in oxygen. Preliminary investigation indicates that this procedure will reduce the O background by a factor of approximately three. Table 1 shows some parameters of interest for incorporating the D_2O and H_2O targets into a fine grained tracker. As a characteristic scale for the water targets will be the order of 0.5 cm, it will be difficult to see recoiling protons with kinetic energy below 30 MeV, so the

majority of the spectator protons will be unobservable. This has little impact on the determination of the neutrino energy but hurts the determination of the transferred momentum.

Reducing the dimensions of the individual water samples clearly allows better selection and specification of those events associated with deuterium, but practical considerations require that it will be difficult to go below 1 cm.

T_p MeV	Q^2 GeV ² /c ²	Range(cm) H ₂ O	Range (cm) STT	P_p GeV/c	RC(m).5T
10	0.0188	0.12	1.2	0.1373	0.916
20	0.0375	0.42	4.2	0.1947	1.299
30	0.0563	0.86	8.6	0.2391	1.595
40	0.0750	1.45	14.5	0.2768	1.847
50	0.0938	2.18	21.8	0.3103	2.070
60	0.1126	3.03	30.3	0.3408	2.273
70	0.1313	4	40	0.3690	2.462
80	0.1501	5.08	50.8	0.3955	2.639
90	0.1688	6.27	62.7	0.4206	2.806
100	0.1876	7.57	75.7	0.4445	2.965
200	0.3752	25.5	255	0.6443	4.299
300	0.5628	50.6	506	0.8079	5.390
400	0.7504	80.9	809	0.9541	6.366
500	0.938	115	1150	1.090	7.272
600	1.1256	152	1520	1.218	8.132
700	1.3132	192	1920	1.343	8.959
800	1.5008	234	2340	1.463	9.762
900	1.6884	276	2760	1.581	10.545
1000	1.876	320	3200	1.696	11.313

Table 4-3: Parameters of water targets for low-density tracking detector

This is a list of important parameters in the design of water targets to be placed in a low-density tracking detector. The 1st column is the proton kinetic energy in MeV. The 2nd is the Q^2 producing T_p assuming the struck nucleon was initially at rest. The 3rd is the proton's range (cm) in water. The fourth is the range (cm) of a proton with T_p in a low density ($\rho=0.1\text{g/cm}^3$) tracker. The 5th is the proton momentum and the 6th is the radius of curvature in a 0.5 T magnetic field.

There is also a possibility that by the time that LBNE is ready to construct the ND, the CCQE cross section on light nuclei, $A \leq 16$, will be known well enough to enable a flux measurement to better than 10% without the use of deuterium. However, there would remain the loss of information of the neutrino energy on an event-by-event basis. A reason for such optimism regarding ν -nucleus CCQE cross sections is the heightened interest in such calculations and a recent awareness of the important role of two-body currents due to meson exchange in the initial state [3,4]. The incorporation of this necessarily more complicated theory into Monte Carlo event generators will involve considerable interaction between knowledgeable theorists and experimentalists.

[1] N. J. Baker et al, Phys. Rev. D23, 2499 (1981)

[2] L. Hulthen, M. Sugawara, S. Flugge (ed.), *Handbuch der Physik*, Springer (1957)

[3] M. Martini, M. Ericson, G. Chanfray, and J. Marteau, Phys.Rev. C81:045502,2010, Phys.Rev.C80:065501,2009

[4] J. Carlson, J. Joudan, R. Schiavilla, and I. Sick, Phys.Rev. C65:024002,2002,

D. Weight, Volume, Magnetic field requirements

The only specification we have at the moment is 1.25 tons of D₂O and 1.125 tons of H₂O. This will take up a volume of 2.375 m³ and will have to be accommodated into a low density tracker.

E. Event rate, Flux specification

The critical event rates are the 35k CCQE events from D and 140K CCQE events from O per year.

F. R&D

The R&D plan for determining the neutrino flux involves extensive simulations of the physics to understand the most effective strategy to introduce D₂O and H₂O targets into the fine grained tracking detector, utilizing the subtraction to determine the neutrino flux. We expect to be given a requirement from the long baseline detector as to how well the flux has to be known to meet their requirements. A considerable effort must then be applied to an optimum design focusing on meeting their requirements with a reliable and cost effective design. Furthermore, we plan to remain in close contact with the group of theorists who calculate ν -nucleus and e-nucleus cross sections to monitor progress in the calculation of absolute CCQE cross sections. The effects of short-range correlations and two-body currents are probably best studied via electron scattering. Thus the possibility of a focused program at Jefferson Laboratory to quantitatively investigate these matters will be investigated.

4.3 Water Target Fine-Grain Tracker (WBS 1.3.4.3)

4.3.1 Scintillator Tracker

A fine-grained scintillator tracker is a candidate near detector. The heart of the proposed detector is a large tracking volume filled with fine-grained scintillator extrusions. Each scintillator has an embedded wavelength shifting fiber to facilitate collection of scintillation light, and every scintillator/WLS fiber channel is individually instrumented with a dedicated photosensor. This detector technology provides full event reconstruction with high resolution tracking capabilities. It is also possible to build up regions of calorimetry by interspersing appropriate absorber material (steel or lead) between sheets of scintillator.

Extruded polystyrene scintillator is not a new concept and has been used successfully in many past experiments. The idea that fine-grained scintillator could be used for a precision tracking detector was first used at K2K in the SciBar near detector. In 2007-2008, SciBar was moved to the Booster Neutrino beam-line at Fermilab and ran as SciBooNE, which studied interaction issues and cross sections of interest to the T2K long baseline program. Fermilab made a significant investment in polystyrene scintillator with the construction of the MINOS experiment. Both the near and far detectors are sampling calorimeters whose active component is extruded polystyrene with a rectangular profile (1.0 cm x 4.1 cm in cross section). Fermilab has an existing extruder line capable of producing modest quantities of scintillator in custom profiles.

Fine-grained scintillator has been a popular choice for near-detector applications as demonstrated in the construction of two new detectors. MINERvA is a new experiment running in the NuMI beamline that is dedicated to studies of neutrino interactions. MINERvA features a large tracking volume of fine-grained scintillator encased in electromagnetic and hadronic calorimetry. It boasts 3 mm vertex resolution and full event reconstruction across a broad kinematic range. Similarly, the T2K 280m near detector features a central tracking region (the P0d) constructed of the same scintillator that was used in MINERvA. As Super Kamiokande is the far detector for T2K, the 280m near detector features interspersed water targets. Scintillator for both experiments was produced on the Fermilab extruder line.

The overall plan for a fine-grained scintillator tracker for LBNE is to re-use large pieces of the MINERvA detector. While the detector will need upgraded downstream hadronic calorimetry and photosensors, a re-configured MINERvA detector is capable of meeting the near detector needs of LBNE. In particular, this fine-grained scintillator tracker will be able to measure the intrinsic ν_e , π , and gamma backgrounds in the neutrino oscillation energy region $E_\nu < 5$ GeV.

This chapter will outline the conceptual plan of a fine-grained scintillator tracker for use as an LBNE near detector. Section 2 will detail the technical design of the detector, including a discussion of how MINERvA will be reconfigured to meet the needs of LBNE. Section 3 will detail infrastructural and personnel needs required to deploy and operate the detector. The last two sections will discuss current R&D plans (Section 4) and the plan for safe implementation of the project (Section 5).

4.3.1.1 Technical Description

In its current incarnation, the MINERvA detector is constructed of 120 planar structures called “modules”. A typical module consists of two sheets of fine-grained scintillator mounted into a hexagonally shaped steel frame. While the steel frame provides the mechanical structure of the module, it is also instrumented and provides hadronic calorimetry for particles exiting out the side of the detector. A typical module contains 302 individually instrumented pieces of scintillator, is 1.5” thick, and weighs just over 3,000 pounds. Modules are hung sequentially on a stand to make up the detector, much as slices make up a loaf of bread. In the downstream regions of the detector, passive absorber material has been interspersed between sheets of scintillator to build up calorimetry regions. The downstream electromagnetic calorimeter is constructed of modules whose scintillator planes have been covered with 2mm-thick lead absorber. The downstream hadronic calorimeter contains modules having only one scintillator plane and a 1” thick steel plate. The very upstream region contains a variety of solid targets (carbon, iron, and lead) embedded in regions of tracking scintillator. The overall layout of the detector structure is shown in Figure ??.

The modular construction of MINERvA also makes the detector reconfigurable. This section discusses how we propose to reconfigure the MINERvA detector to meet the needs of LBNE. We begin by explaining the physics needs motivating the design (Section 2.1), then give an overview of the reconfigured detector (Section ??).

4.3.1.2 Physics Goals of Reconfigured Detector

Chapter ?? of this document discusses the physics goals of the near detector program, including the need to sample the un-oscillated flavor content of the LBNE beam. Of particular interest is the ν_μ , $\bar{\nu}_\mu$, ν_e and $\bar{\nu}_e$ content of the beam. While MINERvA is capable of identifying the lepton in CC final states, separation of ν and anti- ν final states is problematic with the current detector. As configured, MINERvA does not incorporate a magnetic field, so sign determination of the final state lepton is limited. Muons that do not range out in MINERvA may pass downstream into the MINOS near detector, which is magnetized. The threshold for identifying the charge sign of a MINERvA-produced muon with the MINOS near detector is 1.2 GeV. In addition to the obvious kinematic threshold, acceptance for muons entering MINOS falls off for interactions originating in the more upstream regions of MINERvA.

Figure ?? shows simulated far-detector oscillation results for LBNE assuming various combinations of the mixing angles, CP violating phase, and sign of the mass hierarchy. In all cases, the oscillation spectrum has little structure below $E_\nu=500$ MeV. In planning the detector, we wanted to ensure reasonable muon charge sign discrimination for low- E_ν events. Figure ?? shows the fractional energy distribution for muons produced in events having an incident neutrino energy of $500 \text{ MeV} < E_\nu < 1.0 \text{ GeV}$. We set a lower muon charge sign identification threshold in order to ensure reasonable determination of the $\bar{\nu}_\mu$ content of the beam at $E_\nu=500$ MeV.

4.3.1.3 Detector Overview

Our proposed redesign is illustrated schematically in Figure ??. In large part, the detector conserves the existing MINERvA tracking volume and downstream electromagnetic calorimeter. The solid upstream nuclear targets will be removed and replaced with targets more appropriate for LBNE. The most dramatic change is a new downstream hadronic calorimeter. The new HCAL is magnetized and features steel absorber of graduated thicknesses. The following sections provide a few more details for each main detector subsystem.

Targets

In this detector, most of the interactions will occur in the polystyrene scintillator itself. However, other target material can be inserted in between modules, with final state particles being tracked in the surrounding scintillator. As the results of the fine-grained tracker will be most pertinent to a water Cerenkov far detector, water will be the most important target material.

At this point, the design of the water target remains a work in progress. One option is a passive volume of water. The T2K 280m Near Detector incorporates several thin layers of water contained in large plastic bladders. The bladders are distributed throughout the detector's tracking volume, with sheets of tracking scintillator separating target material. The relatively thin targets minimally disrupt the tracking volume. The bladders can be filled and emptied in place, permitting studies of event production on the empty target material. We could implement a similar scheme, perhaps using multi-cellular Lexan sheets.

Christopher Mauger is working on the design of active water targets for use in the near detector program. While the effort is just beginning, the basic idea would be to instrument the water itself, either in liquid form or by production of optical quality ice. Christopher's targets are described in Section ??.

The exact design of the targets, the total volume of water, and its distribution in the tracking volume of the detector remain important issues to be studied.

Tracking Volume

We currently plan to use the existing tracking volume from MINERvA. In its current form, MINERvA dedicates 60 modules to an un-interrupted tracking volume absent of any passive material for targets or calorimetry. This volume encompasses 120 sheets of scintillator, for a total of 15,249 channels, and a total fiducial volume of approximately three tons.

Electromagnetic Calorimetry

This is another system we will keep intact from the current MINERvA detector. The current electromagnetic calorimeter consists of 10 modules, each containing 2 sheets of scintillator. The upstream face of each scintillator plane is covered with a 2mm thick Pb sheet, which serves as the calorimeter's absorber material. Distributed over 20 scintillator planes, there is a total thickness of 4 cm of Pb in the calorimeter.

Magnetized Hadronic Calorimeter

The downstream calorimeter is the first of two major upgrades to the baseline MINERvA detector. The existing calorimeter consists of 20 modules, each containing one scintillator plane and a 1"-thick steel plate. If the current calorimeter were magnetized, the absorber would be too thick to permit lower energy muons to penetrate sufficiently deep into the calorimeter to determine a track curvature, and the sign of the muon.

We are proposing to build a longer, magnetized hadronic calorimeter with graduated steel absorber. The graduated absorber facilitates charge discrimination of lower-energy muons by measuring the track curvature. The calorimeter will be based on the modular construction of MINERvA. The calorimeter modules will still feature a steel frame encasing one sheet of scintillator and a steel absorber plate. The baseline design calls for 15 modules having 1/4"-thick steel absorber, 15 modules having 1/2"-thick absorber, and 15 modules having 1"-thick absorber. A 300 MeV muon originating in the downstream portion of the fiducial volume will be able to cross the first calorimeter region, which should permit determination of the muon's charge. The threshold for traversing the second region (1/2" steel) is approximately 600 MeV. Total energy deposit for a muon traversing the three regions is approximately 1.0 GeV. Muons not ranging out in the calorimeter will still have their charge measured in the hadronic calorimeter, and will pass into the downstream muon catcher for further analysis. 

This calorimeter will require steel and extruded scintillator sufficient to produce thirty additional MINERvA-type calorimetry modules (We plan to re-use 15 of the existing calorimeter modules for the region with 1"-thick absorber.) The calorimeter's magnet will be discussed in Chapter 5.

Downstream Muon Ranger

To further analyze muons passing through the upgraded hadronic calorimeter, we will employ a downstream muon ranger. Our current plan is to employ a subset of the MINOS Near Detector.

Photosensors and Electronics

Because of the calorimeter's magnetic field, we plan to replace MINERVA's Hamamatsu M-64 photomultiplier tubes. We will upgrade the photosensors to some kind of pixelated silicon photodiode, such as MPPCs or SiPMs. Silicon photodiodes are not affected by an ambient magnetic field. They also have the advantage that the higher quantum efficiency will help offset lower production of light from the scintillator as it ages. To simplify readout, we will also replace the old MINOS electronics in the Downstream Muon Ranger. The final detector will employ one single type of photosensor for all instrumented channels.

The upgraded photosensors will also require new front-end electronics. We envision that this will be similar to the current MINERVA design, incorporating an on-board Cockroft-Walton HV supply, eliminating the need for a HV distribution system. Fermilab is currently working on a custom ASIC specifically for silicon photodiodes, and we plan to employ this chip in our front-end boards.

Front-end electronics will be read out by custom interface and timing cards housed in a VME crate. Readout and data acquisition will require a number of dedicated servers. MINERVA employs a C++ based data acquisition software which could be retooled to work with the upgraded detector. In particular, the readout libraries would have to be re-written in order to communicate with the new electronics.

4.3.1.4 Current Design Efforts

The detector description given here is conceptual and requires further studies, optimization, and R&D in order to produce a final design. In its current stage of development, simulations are being used to study the physics capabilities of this detector to determine if it meets the needs of the oscillation program. In general, we are producing efficiencies and purities for the detection of both signal and background reactions in order to understand the detectors performance for comparison to other available detector technologies. As the near detector effort progresses past the conceptual phase, we will further use simulations to refine the design and optimize various detector parameters. Technical issues to be studied in simulation include:

- The amount of target material and its distribution in the detector.
- The thickness of absorber material in the calorimeters.
- The configuration of the magnet for the muon spectrometer. In order to complete a technical design, several issues will need to be addressed through an R&D effort:
 - Selection of the exact photosensor.
 - Mechanical design and testing of the photosensor mount to optimize light collection efficiency.

- Initial design and testing of the front end electronics. R&D plans will be further discussed in Section 4.

4.3.1.5 Infrastructure Needs

Construction and deployment of the LBNE near detectors on the Fermilab site is a large undertaking and will require significant resources, both in terms of personnel and facilities.

4.3.1.6 R&D Needs

While the full R&D program will be discussed later (see Section 4), we will mention here that the R&D program calls for the development of a 1/4 scale sized prototype detector that will eventually serve as our calibration detector. This program will require lab space for on-site assembly of the detector. We plan to run this detector at the Fermilab test beam facility. Following Laboratory policy, we will negotiate a formal MOU with test beam management for access to facilities. For this run, we would like to utilize the tertiary pion beam designed for the MINERvA experiment.

4.3.1.7 Construction Needs

Construction of the downstream hadronic calorimeter will require a large laboratory space with high bay. Construction of MINERvA employed the entirety of Wideband Hall, and a comparable facility will be required. Our requirements for the facility include:

- Approximately 10,000 square feet of floor space. This will permit welding of required module frames, packaging of the scintillator, and construction and source testing of modules.
- Overhead crane coverage with minimum 10 ton capacity covering both the assembly floor and loading dock.
- A loading dock with large access door.
- Sufficient stands for storage of completed modules.

Existing facilities previously constructed for the MINERvA should be re-used. These facilities include detector stands, strongbacks, a large automated radioactive source scanner that was used to test detector modules.

In addition to the surface building, the production of the scintillator will require use of the Fermilab extruder facility.

4.3.1.8 Installation Needs

The deployment of the near detector will require significant infrastructure on the Fermilab site. If pieces of the MINOS near detector will be re-deployed as a downstream muon catcher for the LBNE near detector, then MINERvA must be removed from the MINOS near detector hall first and stored at some surface location prior to being redeployed. This not only permits access to the MINOS near detector, but is required so that the module order is correct in the LBNE near

detector hall (The module order reverses every time that the detector is moved.) From the intermediate facility, modules will be transported to the LBNE surface building, down the shaft and into the near detector hall. Space and facilities are taxed most during detector installation.

While the specific design of the near detector hall and associated surface building will be discussed elsewhere within this CDR, this section will detail needs for the successful deployment and operation of a scintillator tracker near detector.

Intermediate Surface Facility

This intermediate surface facility must meet most of the needs outlined for the construction hall described in Section 3.2, making the construction hall an obvious choice. The LBNE surface building, the near detector hall itself, or some other facility may also be used provided they meet the needs outlined in Section 3.2.

Surface Building

The surface building provides secure access to the shaft and personnel elevators leading to the near detector hall. The surface building must have a high bay capable of staging material to the shaft crane. For this purpose, we prefer the dual overhead crane arrangement previously employed for the MINOS near detector surface building. One crane can be used to offload material off of trucks and move it around the surface building without the access limitations associated with the shaft crane. The high bay must be a minimum of 30 ft high.

As significant amounts of material will be brought down the personnel elevators. We require a minimum aperture of 60 in for all access points to the personnel elevator. This includes all doorways, hallways, and access passages.

During the installation phase, a shaft crane operator and technician crew will be required to move modules during periods of installation. It is hoped that these personnel will be available even during periods of accelerator shutdown.

Finally, we will require access to a van for delivery of instrumentation and lighter material to the surface building.



Near Detector Hall

In order to install the detector, the near detector hall and its access points must be appropriately structured and outfitted. For a MINERvA-like detector, there must be facilities to transport material from the base of the shaft to the near detector hall. At MINOS, this is provided by a cart, which is pushed by a battery powered forklift. A similar arrangement would be suitable for LBNE.

Inside the near detector hall, we have a variety of needs:

- A stand suitable for mounting a MINERvA-like detector: The detector must be mounted so that it intersects the nominal path of the beam through the near detector hall.
- A drip ceiling that suitably covers the experimental area: Ground-water will inevitably seep into the experimental hall through the walls and ceiling of the cavern. Some structure must be

provided that prohibits this water from falling onto the detector, electronics, and other critical pieces of infrastructure. This must be a structure suspended from the rock, which hangs above the level of the overhead crane.

The MINOS near detector hall was originally constructed with a metal roof that covers the MINOS near detector. As experiments were added upstream of MINOS, the metal roof was not extended. Instead, a coating was added to the cavern surface as a lower-cost alternative. The vendor claimed that the coating would react with the ground water in such a way to seal leaks. While the product did slow the seepage of water, it still allows significant persistent leaks, which have affected operation of detectors upstream of the MINOS near detector. This kind of coating should be avoided in the LBNE near detector hall.

Staging area: Open floor space upstream of the detector is required for staging material during installation periods. The minimum floor space required is ??? by ???. The staging area should be covered by the overhead crane.

Room for supporting materials: In addition to the detector, we require room for electronics racks, a table for use while working on the data acquisition PCs, lockers for storing tools and material.

Computer networking: Ethernet access is required for the data acquisition computers. In addition, some facility should exist for personnel to access computer networking, such as an active, spare ethernet port.

Power feeds: Power outlets in convenient locations for the detector and electronics. An articulated personnel lift for use during installation periods.

4.3.1.9 R&D Plans

While much of the detector is to be reused components of the MINERvA detector, the upgraded muon spectrometer and electronics will require a significant R&D effort.

The most pressing need will be selection of photosensors and early design work for the new front-end electronics. This work will be done at Fermilab in conjunction with the Particle Physics Division Electrical Engineering Department. There are several SiPM sensors on the market, and various models will be tested in order to select the most appropriate photosensor for the needs of the LBNE near detector. Once an SiPM has been chosen, early design work for the front end electronics will be carried out and a number of prototype boards will be produced. Work will also begin on techniques for mounting the SiPMs to maximize the light collection efficiency of the detector optics.

Because the muon spectrometer will require production of a significant quantity of extruded scintillator, scintillator will be another key early R&D initiative. We plan to research the production of scintillator with a co-extruded wavelength-shifting (WLS) fiber. The MINERvA construction technique was for the scintillator to be extruded with a hole running the length of the extrusion. The WLS fiber was inserted into this hole when the scintillator sheets were constructed. Optical epoxy was injected into the voids around the WLS fiber to increase optical contact between the fiber and

surrounding scintillator, increasing overall light yields by approximately 30%. As the MINERvA detector was built, all scintillator was source-tested to characterize the detector optics for calibration purposes. This source testing revealed a large weakness in the MINERvA construction technique. In some minority of the channels, the fiber was not completely wetted by the optical epoxy. This imperfect optical coupling produced non-standard attenuation curves for the affected channels. These curves had sudden changes in light levels, which were difficult to parameterize for the calibration effort. A typical affected channel is shown in Figure ???. Insertion of the fiber and injection of the glue was labor intensive, expensive and produced a non-uniform product.

There are also plans to develop a technique whereby the WLS fiber is inserted into the molten plastic while being forced through the extruder die. If successful, the resulting scintillator will provide an overall higher light output and more uniform response.

Finally, as the scintillator and electronics are produced, these elements will be integrated into a small bench-top test setup. A few panels of the new scintillator could be instrumented with the prototype photosensors and electronics. Outfitted with a cosmic-ray trigger, this setup could be used for a number of integration and physics studies on topics such as tracking and calibration of the overall muon energy scale for the scintillator.

Next, parts for a scale model detector would be built. This would be a 1/4-scale size functional detector that would be used to test the upgrades to the standard MINERvA detector. Conceptually, this detector would feature an upstream tracking region of several sheets of fine-grained scintillator. The downstream section would be a small version of the magnetized muon spectrometer.

Components of the detector would be built in the prototype, and it is planned that the component construction would be used for R&D of the construction of the full-sized detector. Groups producing components for the prototype detector would eventually be responsible for producing components for the near detector. This exercise would provide an opportunity to refine construction techniques, train personnel and outfit a production site.

After that, the prototype detector will be assembled and commissioned on-site at Fermilab and will be deployed at the Fermilab test beam facility. The detector components will be 1/4-scale, but will use actual photosensors and a fairly advanced form of the electronics in order to exercise the full readout chain. During commissioning, it will initially trigger on cosmic rays. After that, the detector could be moved to the MINOS Near Detector Hall for some actual neutrino beam running. Finally, it is envisioned that this prototype detector will also serve as a calibration detector.

At this time, any remaining pre-construction R&D, such as production of fixturing for full-sized detector components, revisions to construction protocols based on outcomes from the prototype detector construction, etc., will also be finalized.

4.3.1.10 Safety Concerns

The R&D and construction required to produce this detector will involve exposure to a significant number of hazards. Table 5 lists potential hazards we have identified, possible sources of exposure, and specific steps that can be taken for abating the particular hazards.

Detector R&D and construction will occur both at Fermilab and at collaborating institutions, each of which has their own safety policies. To ensure that work is being properly considered by all institutions, we will require all site managers to perform a safety inventory. Site managers will produce a list of possible safety hazards and review this with institutional safety representatives, and any recommendations must be implemented. A list of hazards and institutional remediation will be provided to the project management before any work is performed.

Aside from the construction process, operation of the detector poses additional risks:

1. **Underground location:** Training will be required for all personnel wishing to access the underground hall for maintenance purposes. Entry will be controlled.
2. **Strong Magnetic Field:** The downstream muon spectrometer will produce a strong magnetic field. The hazard will be posted with specific warning signs, and regions of particularly strong field will be marked. A flashing beacon will signal when the magnet is in operation.
3. **High voltage:** There will be high voltage in the experimental hall. While the use of Cockroft- Walton HV sources for our front-end electronics minimizes any associated risk, the magnet for the downstream muon spectrometer will require an HV supply. The hazard will be posted, and engineered controls will be placed to minimize risk of personnel exposure to this hazard.

Table 5: Hazards associated with construction of the detector.

Hazard	Possible Exposure	Abatement
Radiation	Radioactive sources will be used in the testing and characterization of various detector components.	Follow institutional guidelines for radioactive materials.
Hazardous Materials	Detector construction could involve significant quantities of epoxy or other potentially harmful materials.	Use care when selecting materials; maintain MSDS sheets. Work with institutional safety to determine needs for PPE
Working at Heights	Installation will involve work in an articulated personnel lift.	Training in accordance with Fermilab guidelines.
Work with tools	Detector construction will involve hand and possible power tool usage.	Make PPE available (safety glasses); job specific training provided by supervisors.
Work underground	Detector will be installed in underground experimental hall.	Detector constructed in compliance with Fermilab flammability and toxicity guidelines. Training in accordance with Fermilab guidelines; entry to underground hall will be controlled by procedures similar to those established for the MINOS near detector hall.

4.3.2 Straw Tube Tracker

Another option for the LBNE near detector is to build a high-resolution straw tube tracker detector within a magnetic field. This detector [1] would combine large statistics with high resolution reconstruction of neutrino events. High resolution is imperative to achieve high precision measurements of the neutrino flux and neutrino backgrounds to the oscillation signal in the far detector. The proposed $4 \times 4 \times 7 \text{ m}^3$ detector, inside a dipole magnetic field of $B \approx 0.4 \text{ T}$, will have the density of liquid hydrogen, $\rho \approx 0.1 \text{ gm/cm}^3$, with a nominal fiducial mass of 7.4 tons.

The proposed detector has a clear goal. It is to constrain the systematic uncertainties in the LBNE oscillation measurements. Regardless of the process under study, the systematic error should be less than the corresponding statistical error. Once the precision needed in the ND is established, the focus will turn to the detector parameters that will ensure this precision. To this end, particular attention will be paid to:

- Measurement of the relative abundance and the energy spectrum of the four species of neutrinos in the LBNE beam: ν_μ , $\bar{\nu}_\mu$, ν_e and $\bar{\nu}_e$ via the in situ identification of their CC- interactions.
- Identification and precise measurement of π^0 , photons, electrons and positrons in neutrino-induced neutral-current (NC) and charge-current (CC) interactions (the most important backgrounds to the ν_e -appearance signal in the far detector)
- Measurement of NC cross-sections relative to CC as a function of E_{Had} to establish their dependence on neutrino energy. (NC-processes constitute the largest background to the ν -CC identification)
- Measurement of π^\pm content in CC and NC reactions (the $\pi^\pm \rightarrow \mu^\pm$ decay is the principal background to ν_μ ($\bar{\nu}_\mu$) CC events)
- Quantification of the nuclear-target material cross-sections, which affects the neutrino-nucleus interactions when extrapolating the ND measurements to the FD

The proposed near detector provides powerful constraints on the systematic errors associated with the measurement of the neutrino mixing matrix elements by the LBNE. It promises an “Event-Generator” measurement for the LBNE FD including the hadronic multiplicity (π^\pm , K^\pm , π^0 & p) comprising topologies of CC and NC events with a special focus on the identification of (semi)exclusive e^- , e^+ , γ , relevant to the ν_e appearance. It concurrently offers a precision short-baseline ν -physics program.

The description of the straw tube detector is organized as follows: Section 1 presents the detector concept; Section 2 presents the expected detector performance and sensitivity studies for a select sample of ν -interactions; Section 3 presents the detector dimensions, the power & cooling requirements, and the safety issues; Section 4 presents the planned and anticipated R&D studies.

4.3.2.1 The Proposed SST Detector

The proposed detector has dimensions of $450 \times 450 \times 800 \text{ cm}^3$ embedded in a dipole magnet with $B \approx 0.4 \text{ T}$. The nominal fiducial volume (FV), $350 \times 350 \times 600 \text{ cm}^3$, corresponds to 7.4 tons of mass. A schematic of the straw tube concept is presented in Figure 5; Figure 6 shows the layout with the external muon detector.

The straw tube tracker (STT) idea builds upon the NOMAD-experience [2, 3, 4, 5]. NOMAD is a low-density tracking detector, $\rho \leq 0.1 \text{ gm/cm}^3$, inside a B-field with an electromagnetic calorimeter (ECAL) at the downstream end and, outside the magnet, a muon-detector. We propose an active tracker with a factor of two more sampling points along the z-axis (v-direction) and a factor of six more sampling points in the plane transverse to the neutrino compared to the NOMAD. Figure 7 juxtaposes the resolving power of the NOMAD detector with the massive CCFR/NuTeV calorimeter. One sees the contrast in resolution for an NC event candidate in the NuTeV experiment compared with one in NOMAD. The proposed detector will increase, by an order of magnitude, the data points in tracking charged particles and the coverage for side-exiting neutrals. Taking advantage of the existing design and production details for the ATLAS Transition Radiation Tracker [6, 7, 8] and the COMPASS detector [9, 10], we are proposing straw-tube trackers (STT). Figure 5 is a schematic drawing of one module of the STT. In what follows, we take an STT as a default option for the active neutrino target and tracker. Other technologies could be considered, but we are committed to a low-density, $\rho \leq 0.1 \text{ gm/cm}^3$, precision tracker within a magnetic field. The improvements over the NOMAD detector can be listed. These include:

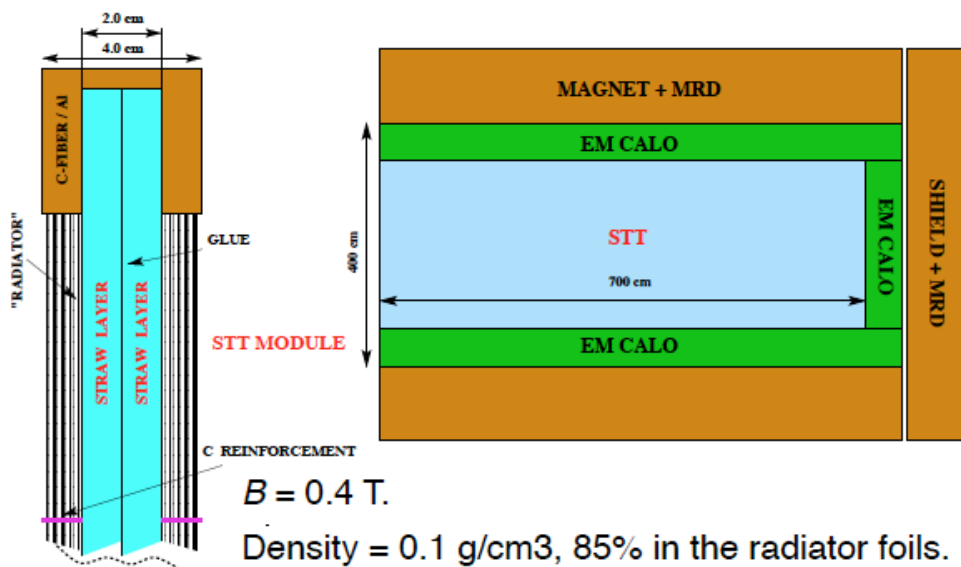


Figure 4-5: Sketch of the proposed Straw Tube Tracker detector

This sketch shows the inner straw tube tracker (STT), the electromagnetic calorimeter (EM CALO) and the magnet with the muon range detector (MRD). The internal magnetic volume is $8 \text{ m} \times 4.5 \text{ m} \times 4.5 \text{ m}$. Also shown is one module of the proposed straw tube tracker (STT). Two planes of straw tubes are glued together and held by an Al-frame. In front of each module a plastic radiator made of many thin foils provides 85% of the total mass of the detector and can be adjusted according to the required resolution and statistics. The module design is taken from the COMPASS experiment.

1) Tracking Detector: The tracker will be composed of straw tubes with 1 cm diameter. Vertical (Y) and horizontal (X) straws will be alternated and arranged in modules - each module containing a double straw layer - as shown in Figure 5. Readout at both ends of the straws to resolve ambiguities in the hit assignment is planned. In front of each module, plastic foils, the “radiators”, provide 85% of the mass and allow a measurement of the transition radiation (TR) which will yield continuous identification of electrons through the tracking volume. Much of active target is composed of carbon. We propose to use Xe-gas in the straw tubes (Xe/CO₂) to maximize the TR capability. Finally, dE/dx will be measured enabling the identification of protons, charged pions and kaons. The identification of individual tracks as protons is especially important for the neutrino Quasi-Elastic (QE) and resonance (Δ) interactions.

(2) Possibly Full Electromagnetic Calorimeter Coverage: The tracking volume will be surrounded by an electromagnetic calorimeter (ECAL) on the four sides and at the downstream end. The ECAL will have transverse and longitudinal segmentation. The default design of ECAL calls for a lead-scintillator calorimeter. In the first stage of construction, only the downstream end of the ECAL and the last 2 m of the sides will be constructed. Later, the tracker could be instrumented completely making the ND fully hermetic. (The granularity will be decided after detailed calculations.)

(3) Improved Muon-Identification: The aim is to tag 95% of the emergent muon in the ν_{μ} -CC sample in contrast with the 85% efficiency in NOMAD. The sides of the dipole magnet will be instrumented with muon-range detector (MRD). Instrumentation in the magnet yoke and the muon detector coverage outside the magnet will enable this improvement (see Figure 2). The muon detectors will be inexpensive RPC's. The muon detector is only meant to provide the identification of the muon — the muon momentum itself will be measured by the STT inside the B-field.

(4) Trigger: Unlike NOMAD, the trigger will not be based upon the geometry or charge-bias. The aim is to have $\approx 100\%$ trigger efficiency for any event with ≥ 100 MeV of visible energy in the tracker or ECAL. 

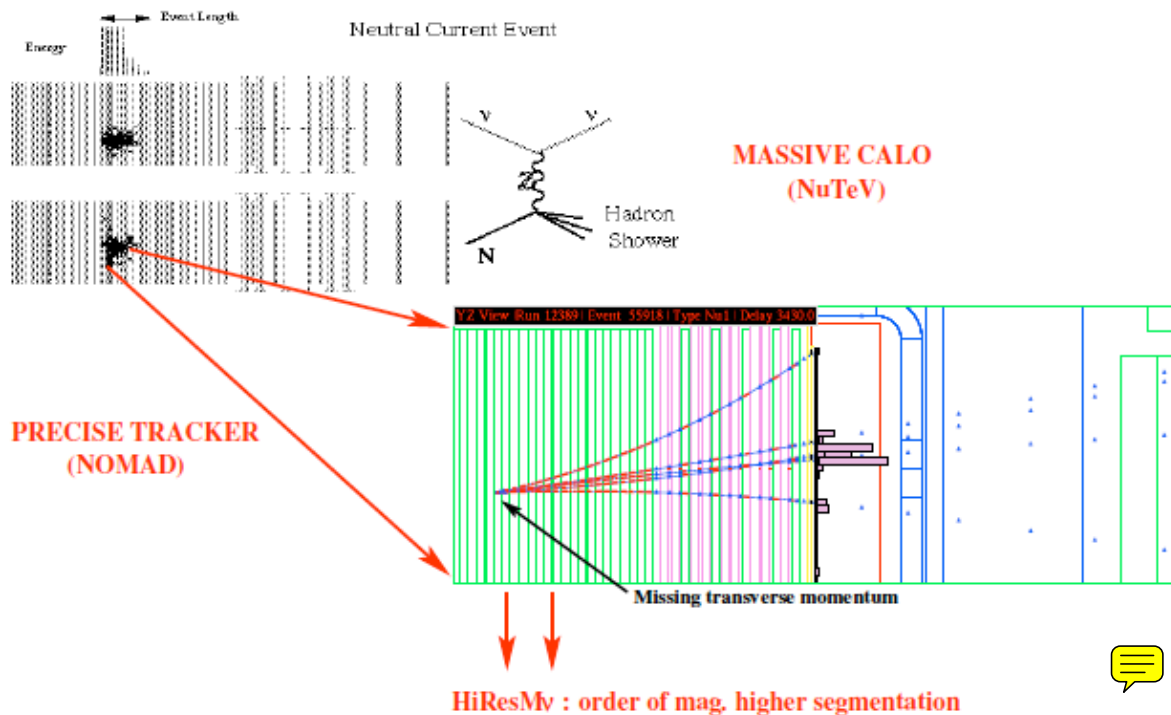


Figure 4-7: Candidate NC event in NuTeV and NOMAD

In tracking charged particles HiResMnu will provide a factor of two higher segmentation along z -axis and a factor of six higher segmentation in the transverse-plane compared to NOMAD.

The energy resolution of the proposed ECAL will be $\approx 6\%/\sqrt{E}$ and a time resolution of 1 ns for electrons and photons with energy ≥ 100 MeV. The muon detector, composed of RPC's, will have a space point resolution of about 200μ and a time resolution of a few nano seconds. The radius of curvature in the magnet will permit a muon-ID down to 200 MeV. The momentum resolution of a $\nu_\mu(\bar{\nu}_\mu)$ -CC induced μ^- (μ^+) is shown in Figure 5 for a 2m long track. It should be noted that the average length of a μ^- (μ^+) track in the SST from a CC is about 3.5m. The energy resolution of a $\nu_e(\bar{\nu}_e)$ -CC induced e^- (e^+) is also shown in the Figure 9 where the electronic charge and direction are measured in the STT and the energy in the ECAL.

A HiResMnu-type ND will measure all four neutrino species: the easily identified ν_μ and $\bar{\nu}_\mu$ CC events with $\geq 90\%$ efficiency, and the more challenging ν_e and $\bar{\nu}_e$ CC with $\geq 50\%$ efficiency with a systematic precision $< 1\%$. Figure 10 shows a ν_μ -CC event in NOMAD, the μ^\pm being easily measured in the tracker with a B-field. The novel feature of a low density detector is a clear measurement of the charged- and neutral-hadrons composing the accompanying hadronic-jet. Figure 11 shows a $\bar{\nu}_e$ CC event, the most difficult of the ν -species to measure, in NOMAD; the e^+ is identified by the curvature, the dotted lines show the bremsstrahlung photons associated with the e^+ -track, the charged- and neutral-hadrons are also identified. The proposed experiment will have substantially better resolution than NOMAD. HiResMv will accurately determine the relative content and E_ν spectrum of all all four ν 's.

Simulations of the proposed HiResMnu detector have been carried out to study the sensitivity to the following processes: (a) ν_e -CC, (b) absolute ν -flux measurement using ν -electron elastic neutral and charged (inverse muon decay) current scattering, (c) π^0 and γ reconstruction in NC, (d) ν_μ -QE, and (e) the shape of the ν_μ and $\bar{\nu}_\mu$ flux as a function of E_ν . The detector simulation is based on a parameterized response of particles. The NOMAD data serve as invaluable calibration for these studies. For each calculation, we conduct an identical simulation using the NOMAD-parameters and checked the results against the NOMAD data and Geant-based MC. Typically, the results agree to within $\pm 15\%$. In the following we summarize these sensitivity studies.

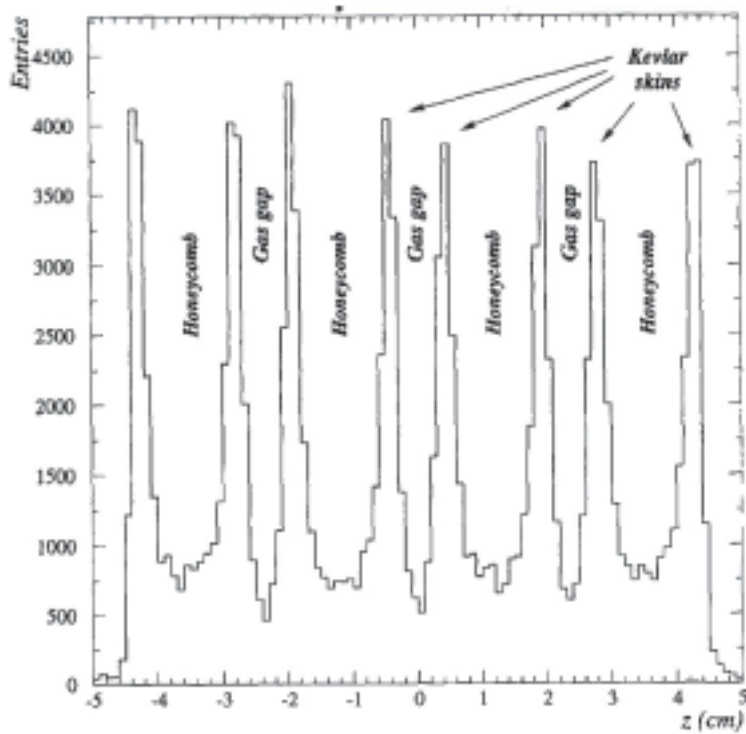


Figure 4-8: A neutrino radiograph of the NOMAD draft chambers

This shows the internal structure of the tracking volume. It illustrates the high resolution of the z -position of the vertex.

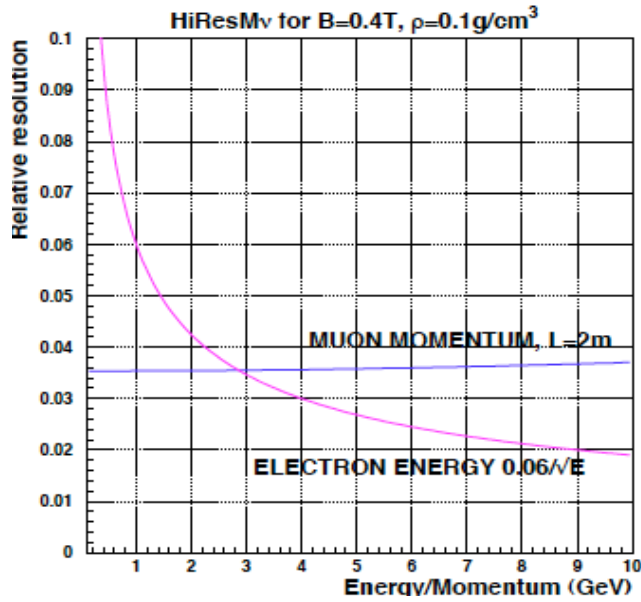


Figure 4-9: Momentum resolution of muons and electrons as a function of momentum
 Muons are shown in blue and electrons in magenta.

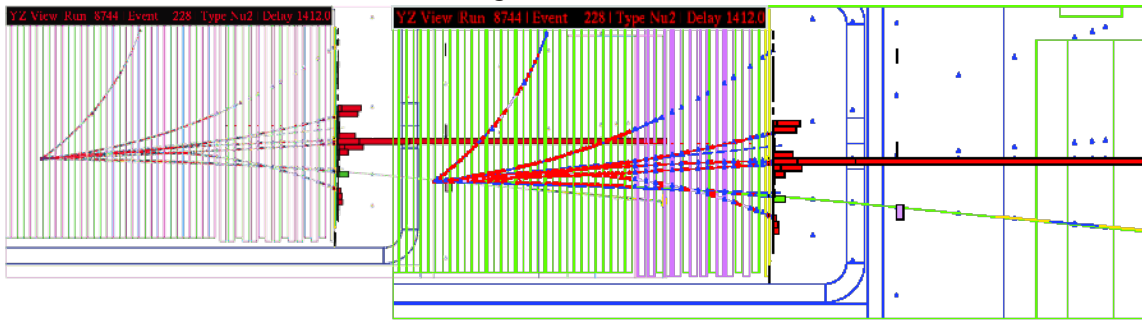


Figure 4-10: A ν_e CC event candidate in NOMAD

The HiResMnu will have more sampling points and better muon coverage.

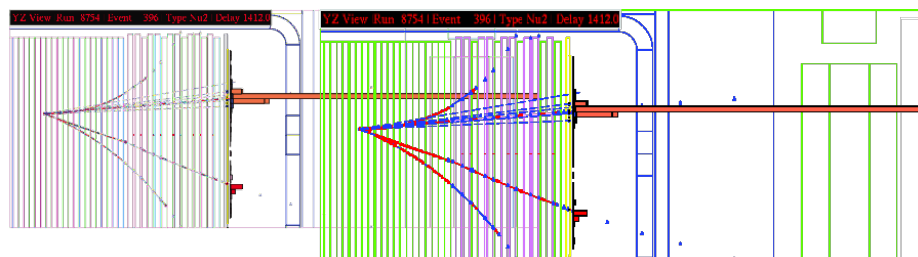


Figure 4-11: An anti-electron neutrino CC event candidate in NOMAD

The positron track with bremsstrahlung photons are clearly visible. The HiResMnu will have more sampling points, TR, and better γ acceptance.

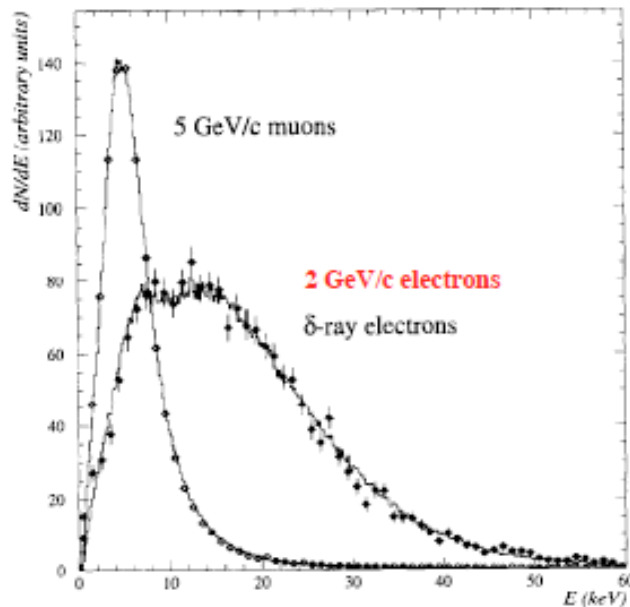


Figure 4-12: Comparison of the TR of a 5-GeV muon and a 2-GeV electron

Sensitivity to ν_e -CC

The goal of this study is to determine the efficiency of $\nu_e(\bar{\nu}_e)$ -CC signal and the reduction of the much larger NC and $\nu_\mu(\bar{\nu}_\mu)$ -CC samples. The relative abundance of $\nu_\mu(\bar{\nu}_\mu)$ -CC:NC: $\nu_e(\bar{\nu}_e)$ -CC is about 1:0.35:0.01. The $\nu_e(\bar{\nu}_e)$ -CC analysis proceeds in two steps. In the first step, we require that there be a negatively charged particle consistent with the electron-TR identification in the event. Figure 12 compares the TR for a 5 GeV muon with a 2 GeV electron as measured by the NOMAD TR-subdetector. Figure 13 shows the electron TR-efficiency as a function of electron momentum for a 10^{-3} rejection of charged pions. Geant simulation of the proposed STT confirms these efficiencies for a 1/1000 pion-rejection. (See DocDB#432-v1.) The surviving background events are completely dominated by an asymmetric photon conversion, producing an actual e^-/e^+ , near the event vertex.

In the second step, the TR-identified electron is required to be kinematically isolated from the hadronic jet. An outstanding feature of STT is the measurement of the momentum vectors in the plane transverse to the ν -direction. Event-by-event determination of the missing transverse-momentum (PTm) vectors offers a powerful tool to constrain the event kinematics, and helps distinguish the NC from CC events, especially when the leading lepton from CC evades detection. The PTm-vector measurement allows a clean separation of NC (non-prompt) from CC (prompt) events. To isolate the ν_e -CC induced prompt- e^- from the NC-induced photon-conversion, we use a multivariate likelihood function built using the momentum vector information of the lepton and the hadron. A mild cut on the lepton versus hadron isolation diminishes the signal efficiency by 10% while reducing the background by 80%. The final efficiency (55% average) and the purity (96%

average) of the ν_e -CC is shown in Figure 14 as a function of the ν_e -energy. The ν_e -CC analysis is conducted in a similar fashion. For the ν_e -CC, if we choose to keep the average efficiency at 50% then the average purity will be 88%.

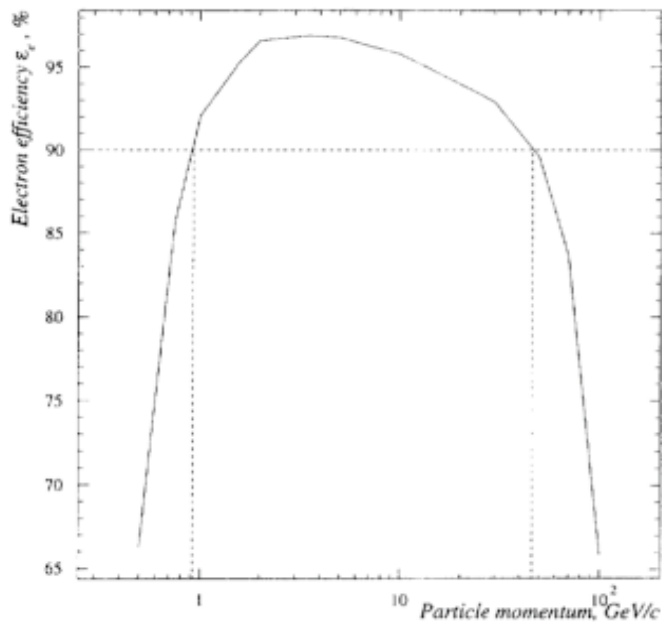


Figure 4-13: Electron TR-ID efficiency as a function of the electron momentum for a 1/1000 rejection of pions

Sensitivity to the Absolute ν Flux Measurement

The proposed ND will offer an in situ absolute ν flux measurement using (a) ν -electron neutral current elastic scattering with an accuracy of $\approx 2.5\%$ for $E_\nu \leq 10$ GeV; (b) ν_μ -electron charged current scattering with an accuracy of $\approx 3\%$ for $E_\nu \geq 11$ GeV (average- $E_\nu \approx 25$ GeV); and (c) the slope of $d\sigma(\nu_\mu - QE)/dQ^2$ on a deuterated target. The three methods are systematically independent. We have studied the first two methods and summarize our findings; the feasibility of the last method is being investigated.

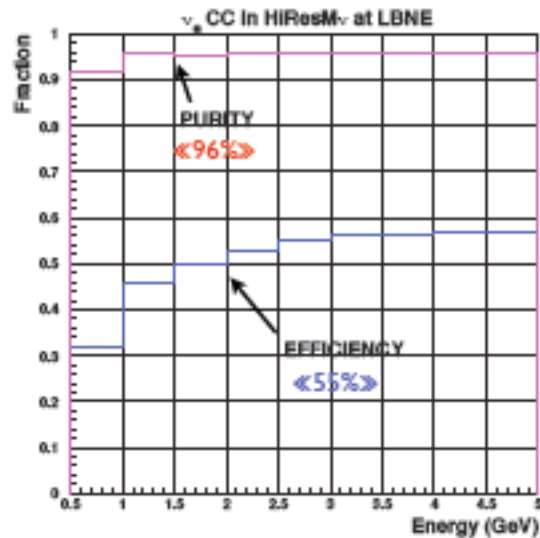


Figure 4-14: Efficiency and purity of the ν_c -CC sample as a function of the ν_c -energy

Absolute ν Flux using ν -Electron Elastic NC Scattering

Using the precise measurement of the weak mixing angle at the Z^0 -pole, the standard model can predict the cross-section of the ν -electron elastic neutral current scattering (NuElas) with $\pm 1\%$ accuracy at the LBNE energies. Therefore, if we could detect NuElas and accurately constrain the background then we can use the SM cross-section to measure the absolute ν -flux. The process unfortunately has a very small cross section, yielding only ~ 560 events per year. To achieve sensitivity to the incident neutrino energy, extremely good angular resolution on the electron momentum is required. However the precisely known cross section and the clean kinematic signature of the process make it a useful constraint on other methods of measuring the neutrino flux.

Absolute ν Flux using Inverse Muon Decay

Inverse muon decay (IMD), $\nu_\mu + e^- \rightarrow \mu^- + \nu_e$, offers an elegant way to determine the absolute neutrino flux. Given the μ^- threshold, however, IMD requires a minimum neutrino energy of $E_\nu \geq 10.8$ GeV. Over a three year period, the STT detector should see ~ 300 IMD events. The reconstruction efficiency of the single, energetic, and extremely forward μ^- is $\geq 98\%$. The angular resolution of the IMD- μ is ≤ 1 mrad. The background, primarily from the ν_μ -QE, is negligible and will be precisely measured. We anticipate that the IMD events will allow the absolute neutrino flux at high energies to be determined to $\sim 5\%$ precision.

Sensitivity to the π^0 , γ , and π^\pm Identification

The principal background to $\nu_e(\bar{\nu}_e)$ -appearance comes from the NC π^0 events. The proposed ND is designed to measure π^0 's with high accuracy in three topologies: (i) both photons convert in the tracker ($\approx 25\%$); (ii) one photon converts in the tracker and the other in the calorimeter ($\approx 50\%$); and (iii) both photons convert in the calorimeter. The first two topologies afford the best resolution, as the tracker provides accurate γ -direction measurement.

Based on NOMAD experience and the improved resolution of the STT, the proposed STT detector is designed to have substantially improved photon reconstruction ability down to 80 MeV.

To estimate the π^0 reconstruction efficiency, we focused on events where at least one photon converts in the STT. Figure 15 shows the π^0 reconstruction efficiency as a function of π^0 energy for NC events. Including photons that reach the ECAL, the reconstruction efficiency is expected to be $\geq 75\%$. Figure 16 shows the reconstructed photons in the NOMAD NC sample. Improvements in the STT π^0 reconstruction comes from two considerations: first, 50% more photons will convert in the tracker; second, the e^-/e^+ track will have a factor of 12 more track points than that in NOMAD, enabling more efficient reconstruction of low momenta e^- and e^+ . Finally, the combinatorial background will be much smaller in LBNE than NOMAD.

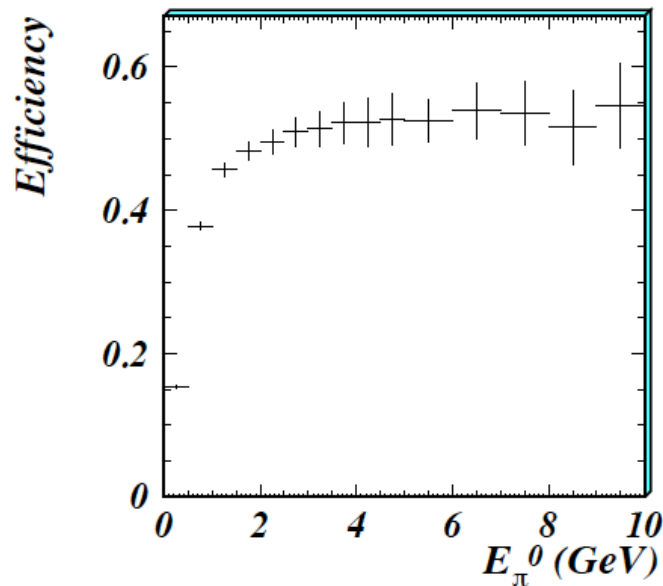


Figure 4-15: π^0 reconstruction efficiency as a function of π^0 energy for NC events.

The discussion above also implies that the reconstruction of events with exclusive single photons will be straightforward. Exclusive photon events occur rarely since to first-order, photons appear in pairs from π^0 -decay in ν -interactions. If processes exist that produce single photons, then 50% of these will be cleanly reconstructed in the proposed STT. The proposed detector will have better resolution to reconstruct π^0 than NOMAD and will completely determine the π^0 -CC- and π^0 -NC-induced photons, exclusive and semi-exclusive, as functions of energy and angle with high purity. By contrasting the π^0 mass in the tracker versus the calorimeter, the relative efficiencies of photon reconstruction will be well constrained.

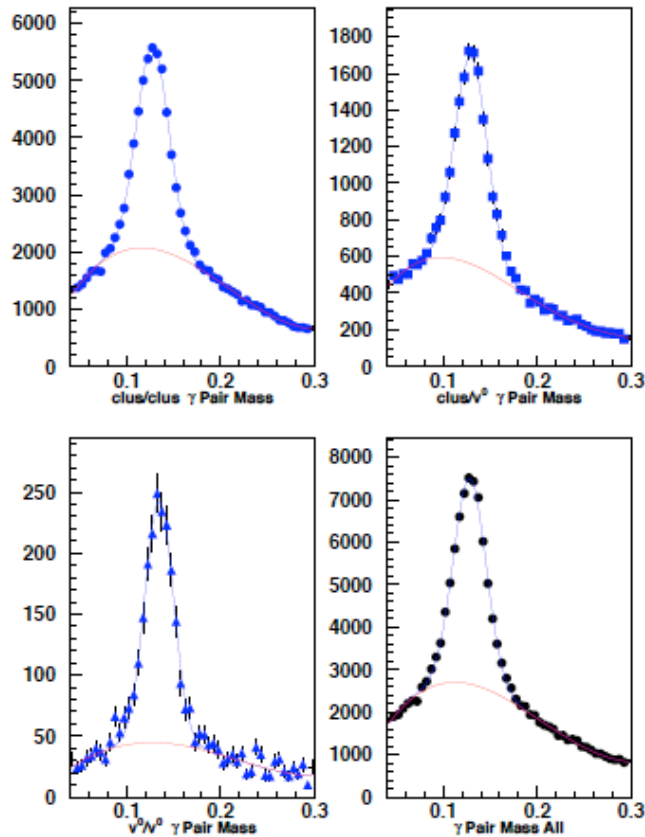


Figure 4-16: Reconstruction of π^0 in inclusive NC events in NOMAD (preliminary).

Finally, the π^\pm will be measured by the tracker, including the dE/dx information. An in situ determination of the charged pions in $\nu_\mu (\bar{\nu}_\mu)$ -CC events, with and without μ ID, and ν -NC events is crucial to constrain the systematic errors associated with $\nu_\mu (\bar{\nu}_\mu)$ -disappearance, especially at low-Ev. The STT determination of charged pion production in non- μ ID-CC and NC will all but eliminate this error. The NOMAD event pictures of $\nu\mu$ -CC, νe -CC and NC show that the measurement of the charged hadrons in the proposed STT will be routine.

Sensitivity to $\nu\mu$ -QE

In the LBNE physics program, quasi-elastic (QE) events are essential as the LBNE oscillation signal occurs at energies where QE dominates. A measurement of $\nu\mu$ -QE provides, to first order, a measurement of flux. Because of the simple topology of a QE event — just a μ^- and a proton — the interaction provides direct information on initial state Fermi momentum and final state interaction (FSI) dynamics. Much can be learned from $\nu\mu$ -QE by measuring the two-track (μ -p) topology. The experimental challenge is the reconstruction of the emergent proton. The STT is designed to accurately and efficiently identify the proton and measure its momentum vector. The

STT will have the ability to measure the “dE/dx” of the recoil proton. The efficiency of reconstructing the proton will be twice that of NOMAD. By contrasting the 2-track topology with the 1-track topology (which is what most experiments measure), one can obtain an in situ measure of the Fermi-motion. Furthermore, the two track topologies are very sensitive to the FSI parameters. By demanding consistency in the cross-section between the two topologies, the nucleon Fermi motion and the FSI parameters can be constrained. The degree that such reconstruction can allow the selection of events from deuterium rather than oxygen from a D₂O target is a matter for future study. Figure 17 shows the efficiency and purity of reconstructing $\nu\mu$ -QE induced μ -p events as a function of E_ν in LBNE.

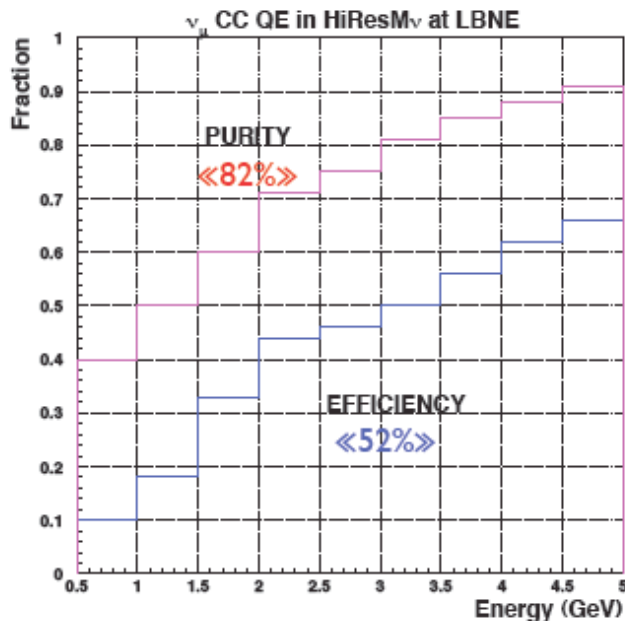


Figure 4-17: Efficiency and purity of ν_μ -CC QE scattering in the proposed STT

The ν_μ and $\bar{\nu}_\mu$ Flux as a Function of E_ν and FD/ND Prediction

A promising method to determine the shape of the ν_μ and $\bar{\nu}_\mu$ fluxes is by measuring CC events with low-hadronic energy (ν)— the low- ν_0 method of relative flux determination [11]. In this analysis, the key quantities are the resolution for low- ν events and the systematic precision of the muon-momentum measurement. The ν_μ ($\bar{\nu}_\mu$)-CC flux provides a measure of the $\pi^+/K^+/\mu^+$ ($\pi^-/K^-/\mu^-$) content of the beam. Following the NOMAD analysis, we first obtain the relative ν_μ ($\bar{\nu}_\mu$)-flux at the ND. Next, we fit the $d^2\sigma/dx_F dP_T^2$ of the parent mesons to the ν_μ -flux. The ingredients to the empirical fit to the meson production cross-section (EP) are the measured ν_μ -flux at the ND, constraints from hadro-production experiments (MIPP), and the simulation of the beam transport. The systematic error analysis includes ν_0 -correction, composition of CC (QE .vs. Resonance .vs. transition-region .vs. DIS), muon energy scale, low hadronic energy resolution, beam-transport errors and different functional forms. Calculations indicate that a high resolution

near detector will reliably predict the FD/ND to $\leq 2\%$ precision as a function of Ev, and a ND at 500m can predict the FD/ND flux just as precisely as a ND at 1000 m.

An accurate measure of $\nu_\mu (\bar{\nu}_\mu)$ -CC events provides an absolute prediction of the ν_e -content of the beam. The reason is that the $\nu_\mu (\bar{\nu}_\mu)$ CC-spectrum provides a measure of the $\pi^+/K^+/\mu^+$ ($\pi^-/K^-/\mu^-$) content of the beam, and the ν_e -CC provides a direct measure of K_L^0 s, an elusive source of ν_e s.

The above presents a concept of an absolute measurement of LBNE ν -flux with the proposed STT. The program includes an absolute flux determination using CCQE events and ν -electron neutral and charged current interactions. The ultimate precision on the absolute flux will be $\leq 5\%$. The ND will measure the ν_μ , $\bar{\nu}_\mu$, ν_e and $\bar{\nu}_e$ CC-spectra. Using the low- ν_0 flux technique and the empirical parameterization of the π^\pm , K^\pm , K^0 , and μ^\pm , one can predict the FD/ND $\nu_\mu (\bar{\nu}_\mu)$ flux ratio with $\leq 5\%$ precision in Ev bins.

4.3.2.3 ND Hall and Infrastructure Needs

Dimensions, Mass and Detector Stand

The specifications for the proposed near detectors are shown in Table 4-4.

Item	Specification
Inner magnetic volume	8 x 4.5 x 4.5 m ³
STT	3.5 x 3.5 x 7 m ³ (160 modules)
ECAL	50 cm thick
Thickness of Cs and Coils	1.3 m
Muon Range Detector (MRD)	Iron ("C") of the dipole RPC-instrumented
External Muon Detector	ID for high-energy (>2.5 GeV) muons

Table 0-1: Specifications for the proposed near detectors

Power Requirements

The main requirement in terms of power consumption comes from the dipole magnet. The power required to run the UA1 magnet at a nominal field of 0.4 T, corresponds to about 1.7 MW. Using copper coils instead their AL coil lowers the power requirements to about 1.04 MW at the nominal field of 0.4 T.

For the STT power consumption, the power measured in the ATLAS TRT detector is used since the readout chain is essentially the same in STT. The total number of channels in the ATLAS TRT, including both barrel and end-cap detectors, was about 350,000, for a total power consumption of about 44 kW. The SST will have 112,640 straws with readout at both ends, giving a total of 225,280 electronic channels and an estimated power consumption of about 28 kW. The ECAL portion of the detector is expected to have about 50,000 channels by scaling the corresponding numbers for the T2K ND280 detector. Assuming the same power consumption per channel as the STT, this would translate to an additional 6 kW. Finally, for the muon system the estimated power requirement is about 15 kW.

The total power required to run the proposed STT detector is therefore expected to be about 1.1 MW with the nominal field configuration of 0.4 T. Assuming we run continuously, 365 days/year, and a nominal cost of the electricity of \$0.08/kWh, the power consumption will cost about \$771,000/year.

Cooling Requirement

The cooling of the dipole magnet requires a water flow of about 30 liters/s to dissipate the heat produced by the current circulating in the copper coils.

The cooling of the muon system, located outside of the magnet, can be achieved by natural convection in the near detector hall. The main cooling requirements are related to the sub-detectors to be installed inside the dipole magnet. To this end, we can use the same cooling system as in the ATLAS end-cap TRT. The STT detector requires an overall CO₂ envelope of gas acting as a barrier between the active part of the detector (the straws) and the environment, to prevent the effect of moisture and other sources of pollution. The cooling of the STT detector requires the operation of a dedicated cooling gas system providing CO₂ flow rates of 100m³/h. Alternately, a standard mono-phase cooling system using a room-temperature C₆F₁₄ fluorinert coolant can be used, coupled with heat exchangers on the STT frames and the front-end electronics boards. The cooling of the ECAL detector can use the same cooling system as the STT.

Staging Area & Electronics

Safety Issues

No major safety issues are present for the proposed STT detector. All gases used are non-flammable. The main gas system feeding the straws is a closed recirculating system. The total gas volume present inside the straws is about 39m³. The overall outer envelope of the STT detector is about 78m³ and must be sealed from the outside by flushing CO₂. A possible issue is the leak of CO₂ into the near detector hall.

Safety valves must be installed for the STT at the outer edges of the gas seal to prevent the differential pressure between the inside of the STT volume and the outside from exceeding ± 0.5

mbar. More than 3,000 temperature sensors will be distributed in the STT to monitor the temperature of the active detector, as well as that of the front-end electronics and of the cooling circuits. In addition, many parameters of the closed-loop active gas system will be monitored. The gas gain will be continuously measured by a set of reference straws located outside the STT volume, and an automated algorithm will adjust the high voltage on the detector to preserve the stability of the gas gain as the environmental parameters (temperature and/or pressure) change.

4.3.2.4 R&D Studies

The main sub-detector in the proposed SST is the Straw Tube Tracker, which is also the one in the most advanced design stage. The technology used for this detector is well established and already operational in the ATLAS and COMPASS experiments at CERN. The detailed design of the STT modules is a simple modification of the tracker structure of the constructed wide-aperture magnetic spectrometer in COMPASS. The COMPASS straw tracker uses straws of the same diameter (10mm) and has a sensitive area of $3.2 \times 2.8 \text{ m}^2$, which is very similar to the one in SST. In addition, we combine the tracking capability with the particle identification by measuring both drift times and energy loss, as in the ATLAS TRT detector. The readout electronic chain and the use of radiators for the Transition Radiation follow closely the ATLAS design. The cost estimate for the STT part of the detector is based upon the actual costs of the ATLAS TRT (straws, 23 radiators, assembly, readout chain, gas system) and of the COMPASS straw tracker (mechanical frames). Updated quotes from the same vendors who supplied the parts for the ATLAS TRT have been obtained. With the help of the JINR laboratory in Dubna, Russia, which was one of the production centers for both the ATLAS TRT and the COMPASS straw tracker, we prepared a detailed cost estimate including all items needed for the construction of the actual detector. It must be noted that straw modules very similar to the ones foreseen for this proposal have already been built and used in several detectors.

For the dipole magnet we use the UA1 magnet as reference (also used by NOMAD and T2K ND280), and we scale the corresponding dimensions to the magnetized volume required by STT. Our cost estimate is based upon the actual costs of two large aperture dipole magnets built for experiments at CERN: a) the UA1 dipole magnet and b) the more recent LHCb dipole magnet. It is interesting that the costs of these two existing magnets, which have comparable magnetized volumes, are similar, in spite of the different designs and the long period of time elapsed between them. The designs of both the UA1 and the LHCb dipole magnets are significantly more complex than the one foreseen for STT, due to special requirements on the field shape and field strengths. Another important element to consider is the maximal field B_{max} achievable, as the cost is roughly proportional to the value of B_{max} . The nominal field in STT will be 0.4 T, but we plan to design the magnet with $B_{\text{max}} \sim 0.6 \text{ T}$ in order to allow some flexibility on the detector parameters. This value is lower than the B_{max} of both UA1 (0.7 T) and LHCb (1 T) magnets. However, the total magnetized volume is larger in SST ($4.5 \times 4.5 \times 8 \text{ m}^3$) than in the UA1 magnet ($3.5 \times 3.5 \times 7 \text{ m}^3$) by a factor of 1.9.

The design of the electromagnetic calorimeter (ECAL) is still under development since to date the focus has been on the STT. For the cost estimate we use as a reference the electromagnetic calorimeter built for the T2K ND280 detector, which was mounted inside the UA1 magnet and has a geometry similar to that of the SST. The T2K calorimeter is a lead-scintillator sampling

calorimeter, 10 radiation lengths (X_0) thick, which if instrumenting both the sides of the UA1 magnet and the forward region, provides hermetic coverage of the detector. Due to the higher neutrino energy in LBNE compared to T2K, a deeper ECAL is required, from $10X_0$ to about $18X_0$, depending upon the longitudinal position inside the magnet. Therefore, the costs of the T2K design are scaled both by the total area to be instrumented and by the increased thickness. It must be noted that the total area covered by the sides is about 120m^2 , while the area of the forward ECAL region is only 16m^2 . The large ECAL area required to fully instrument the sides of the magnet implies the overall cost of ECAL is dominated by this part. However, the instrumentation of the ECAL sides is also more problematic due to the lower average energy of the photons, the presence of material from the STT frames in front of the side ECAL and the higher pile-up rates from events occurring in the return yoke of the magnet. It seems therefore reasonable to stage the construction of the ECAL and/or to partially instrument the sides of the magnet with ECAL. The highest priority should be given to the forward ECAL, followed by the downstream region of the magnet sides. Our cost estimate assumes the instrumentation of the forward region and the sides for the last downstream 3m with an ECAL of $18X_0$ constant thickness.

For the muon system we have only a conceptual design based upon the NOMAD experience for the moment. The main differences between the proposed STT and NOMAD are that the sides of the magnet are to be instrumented in addition to the forward region and that we will use inexpensive RPCs instead of drift chambers.

The primary task of HiResMnu is to reduce systematic uncertainties in the neutrino oscillation searches performed by the LBNE at DUSEL. Concurrently, the proposed SST ND will offer a generational advance in the precision searches and measurements in neutrino physics. To this end, the high resolution tracking capability within a light target, the presence of the magnetic field, and electron-ID are the three crucial ingredients. The optimization of the detector performance and of the sensitivity to oscillations achievable by the LBNE will require detailed simulations. We plan to study the physics potential of HiResMnu by performing a full simulation of the detector response and of the physics processes expected in neutrino interactions. We shall validate our detector simulations against the results of the STT test beam exposure. We will also use the existing neutrino data from the NOMAD experiment to cross-check our results and simulations of neutrino interactions. To establish the SST concept and optimize the detector design, tasks in order of priority are listed below.

Simulation Studies

We need a detailed GEANT based simulation of the proposed detector and various options. Thus far, we have used a parameterized fast simulation. Fortunately, the NOMAD data serve as a very important calibration for the calculation. These data will continue as an important guide in the simulation studies.

A Full Scale STT-Module Construction

One full scale STT module is planned to be built during the R&D work. We do not anticipate exposing the full scale module to the test beam. However, it is important to establish the detailed modus operandi for the mass production of STTs.

ECAL Prototype

Our default ECAL design is based upon the lead-scintillator calorimeter used in the T2K-ND280 detector. For ECAL, the most important region is the downstream end of the detector — we propose to build this in the first stage. The ECAL will have transverse and longitudinal segmentation. We propose to build a $10 X_0$ deep calorimeter with lead (1.75mm) and scintillator (4cm x 1cm) sampling in the downstream region. In the second stage, we plan to instrument the sides, $5 X_0$ deep with coarser granularity which will make the detector hermetic. The ECAL R&D effort will begin a year after STT, and two years after simulation studies, and will last about two to three years.

Dipole Magnet



The proposed dipole magnet is a larger version of the UA1 dipole magnet used by NOMAD. Figure 16 shows the magnet yoke assembly, Figure 17 shows the yoke & coils, and Figure 19 shows the coil assembly. Table 6 summarizes the salient parameters of this magnet at maximum operating B-field of 0.6 T. The SST magnet will operate at $\sim 0.4T$.

The main differences between the UA1 and the SST magnet are: (a): Size; (b): Coil — UA1 used Al-coil (to minimize the degradation of the energy resolution of the outgoing jets) with resistivity $\rho_{Al} = 2.8 \times 10^{-8} \Omega m$, whereas the SST will use Cu-coil with conductivity $\rho_{Al} = 1.7 \times 10^{-8} \Omega m$; and (c): SST magnet does not need a hole in the coil as was the case with the UA1 magnet.

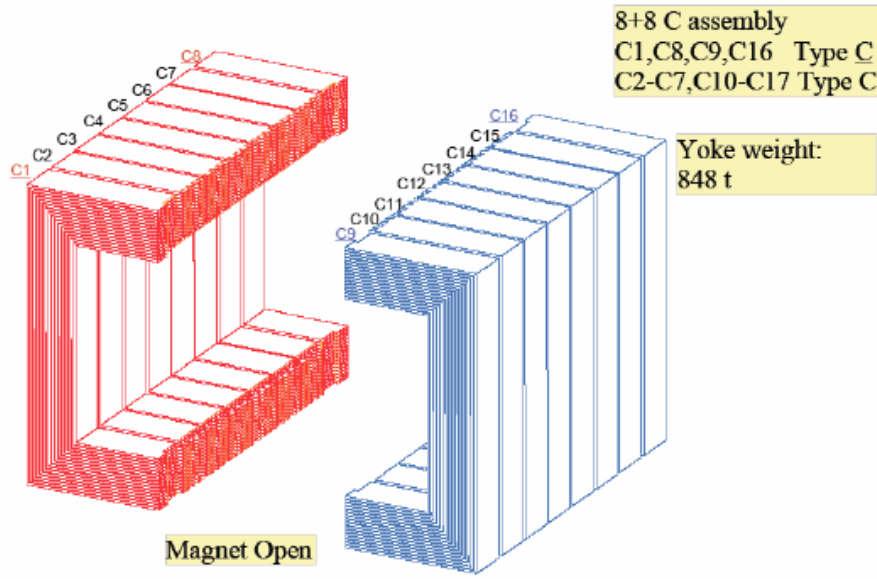


Figure 0-1: Magnet yoke assembly of the UA1 dipole magnet

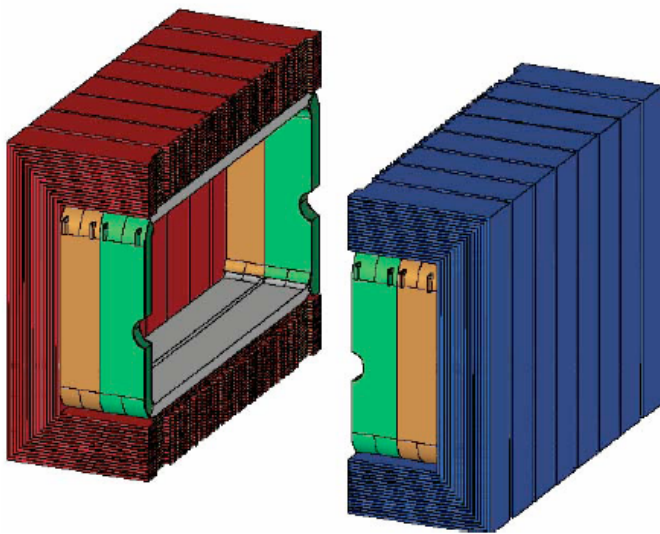


Figure 0-2: Yoke and coil of the UA1 dipole magnet

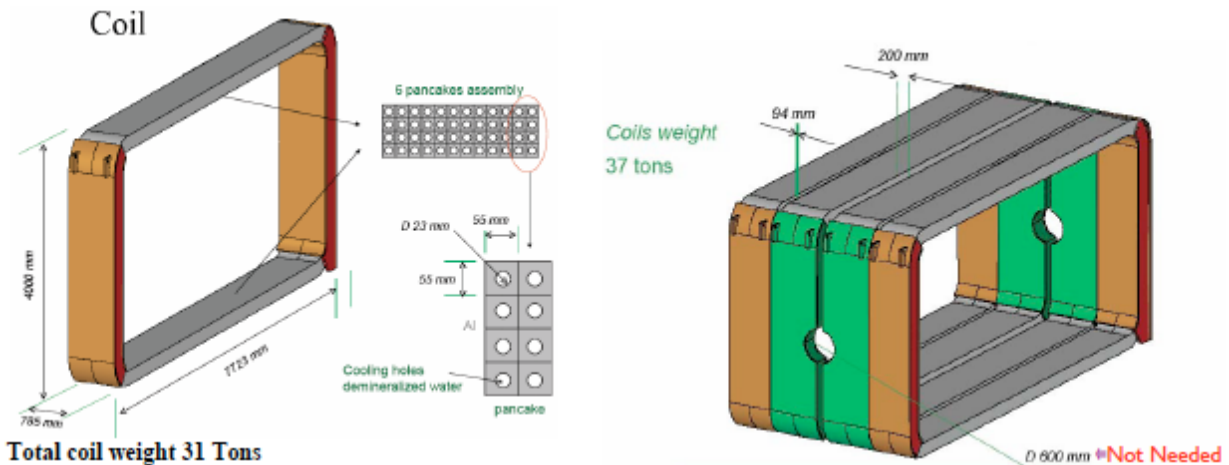


Figure 0-3: Coil and coil-assembly of the UA1 dipole magnet

The main differences between the UA1 and the SST magnet are: (a): Size; (b): Coil — UA1 used Al-coil (to minimize the degradation of the energy resolution of the outgoing jets) whose resistivity $\rho_{Al} = 2.8 \times 10^{-8} \Omega m$ whereas the SST will use Cu-coil whose conductivity is $\rho_{Cu} = 1.7 \times 10^{-8} \Omega m$; and (c): SST magnet does not need a hole in the coil as was the case with the UA1 magnet.

Muon Detector

In the proposed design, the muon detectors will identify muon tracks, which will then be matched with the STT tracks with measured momenta and charges. The muon detectors are not required to furnish muon momentum, only the μID . However, given the large muon rate in the ND location, μ -detectors with good spatial ($\approx 200 \mu m$) and time (\approx a few ns) resolution are needed to provide a good match with the STT tracks.

Two types of muon detectors will be employed in the proposed detectors. First, we plan to instrument the magnet yoke with the muon-range detectors (MRD), which will offer μID at low momentum, down to 200 MeV. Second, there will be large muon detectors outside the magnet at 5λ and 8λ , respectively, to identify the high-energy muons. (NOMAD only used the large muon detectors outside the magnet.)

Inexpensive RPC's are the choice of the muon-detectors. Our calculations show that they will survive the rate and provide the μID with adequate precision. The R&D effort will begin concurrently with the ECAL work, about two years after the simulation studies.

References

- [1] [hiresmnu] S. Mishra, R. Petti and C. Rosenfeld, Letter of Intent submitted to Fermilab, February 2008, http://www.fnal.gov/directorate/Longrange/Steering_Public/community_letters.html;

S. Mishra, R. Petti and C. Rosenfeld, Proceedings of the Nufact08 conference - Valencia Spain, June 30 - July 5 2008, PoS SISSA 069 (2008), arXiv:0812.4527 [hep-ex]; to be submitted to NIM.

- [2] [NOMADnim] J. Altegoer et al. [NOMAD collaboration], Nuclear Instruments and Methods A 404 (1998) 96-128.
- [3] [NOMAD-nmnt] P. Astier et al. [NOMAD collaboration], Nucl. Phys. B611 (2001) 3-39, hep-ex/0106102
- [4] [NOMAD-nmne] P. Astier et al. [NOMAD collaboration], Phys. Lett. B 570 (2003) 19-31, hep-ex/0306037
- [5] [NOMAD-cohpi0] C.T. Kullenberg et al. [NOMAD collaboration], submitted to Phys. Lett.B; arXiv:0910.0062v1 [hep-ex]
- [6] [ATLAS-TRT1] T. Akesson et al., Nucl.Instrum.Meth. A522 (2004) 131-145
- [7] [ATLAS-TRT2] T. Akesson et al., Nucl.Instrum.Meth. A522 (2004) 50-55
- [8] [ATLAS-TRT3] T. Akesson et al., IEEE Nucl.Sci.Symp.Conf.Rec.2 (2005) 1185-1190
- [9] [COMPASS-straw1] V.N. Bychkov et al., Particles and Nuclei Letters, 2 (111) June 2002
- [10] [COMPASS-straw2] K. Platzer et al., IEEE Transactions on Nuclear Science, vol. 52, No. 3, June 2005
- [11] [Mishra-nu0] S.R.Mishra, Review talk presented at Workshop on Hadron Structure Functions and Parton Distributions, Fermilab, Apr.1990; World Scientific, 84-123(1990), Ed. D.Geesaman *et al.*; Nevis Preprint # 1426, Jun(1990);
- [12] [NOMAD-CCV0] P. Astier et al. [NOMAD collaboration], Nucl. Phys. B621/1-2 (2001) 3-34, hep-ex/0111057
- [13] [NOMAD-NCV0] D. Naumov et al. [NOMAD collaboration], Nucl.Phys.B 700 (2004) 51-68, hep-ex/0409037
- [14] [NOMAD-xsec] Q. Wu et al. [NOMAD collaboration], Phys. Lett. B 660 (2008) 19-25; arXiv:0711.1183 [hep-ex]
- [15] [PDG06] Particle Data Group, W.-M. Yao et al., Journal of Physics, G 33 (2006) 1
- [16] [nutev-sin2w] G. P. Zeller et al. [NuTeV collaboration], Phys. Rev. Lett. **88**, 091802 (2002), arXiv:hep-ex/0110059.
- [17] [pw-R-] E. A. Paschos and L. Wolfenstein, Phys. Rev. D **7**, 91 (1973).
- [18] [marciano00] A. Czarnecki and W.J. Marciano, Int. J. Mod. Phys. A15 (2000) 2365
- [19] [APV-sin2w] S.C. Bennet and C.E. Wieman, Phys. Rev. Lett. 82 (1999) 2484
- [20] [E158-sin2w] P.L. Anthony et al [E158 collaboration], Phys.Rev.Lett. 95 (2005) 081601, hep-ex/0504049
- [21] [nutev-2muanomaly] T. Adams et al. [NuTeV collaboration], Phys.Rev.Lett. 87 (2001)

041801, hep-ex/0104037

- [22] [miniboone-osc] A.A. Aguilar-Arevalo et al. [MiniBOONE collaboration], Phys. Rev. Lett. 98 (2007) 231801, arXiv:0704.1500 [hep-ex]
- [23] [miniboone-sergey] S. Gninenko, arXiv:0902.3802 [hep-ph]
- [24] [ssbar] S. Alekhin, S. Kulagin and R. Petti, arXiv:0812.4448 [hep-ph], Physics Letters B 675 (2009) 433-440.
- [25] [AKP-proc07] S. Alekhin, S.A. Kulagin and R. Petti, AIP Conf.Proc. 967 (2007) 215-224, arXiv:0710.0124 [hep-ph]
- [26] [AKP-nuint07] S. Alekhin, S.A. Kulagin and R. Petti, Nuint 07, Fermilab, Batavia, May 30 – June 3 2007, talks in <http://conferences.fnal.gov/nuint07/>
- [27] [DIS08] S. Alekhin, S.A. Kulagin and R. Petti, Proceedings of DIS08 - University College London, April 7-11 2008; arXiv:0810.4893 [hep-ph].
- [28] [Arbuzov-Bardin] A. B. Arbuzov, D. Y. Bardin and L. V. Kalinovskaya, JHEP **78**, 506 (2005); arXiv:hep-ph/0407203.
- [29] [Dittmaier] K. P. Diener, S. Dittmaier and W. Hollik, Phys. Rev. D **69**, 073005 (2004).
- [30] [KP-01] S.A. Kulagin and R. Petti, Nucl. Phys. A 765 (2006) 126-187, hep-ph/0412425
- [31] [KP-02] S.A. Kulagin and R. Petti, Phys.Rev. D 76 (2007) 094023, hep-ph/0703033

4.4 Liquid Argon TPC (WBS 1.3.4.4)

4.4.1 Requirements and Specifications

As already described in the introduction and in section 4.1, the near detectors are required to measure the interaction rates of each flavor of neutrino and antineutrino. These should be measured separately for each flavor, as a function of neutrino energy. Special care must be taken to identify interactions of non-electron-flavor neutrinos and antineutrinos that mimic electron-flavor interactions, especially neutral-current interactions producing π^0 mesons or photons. This last requirement mandates good resolution of individual tracks within the detector at the sub-cm level.

If all neutrino interaction cross-sections were known for all isotopes with great precision, any detector capable of making the flux measurements described above would be equally suitable for use as a near detector. However, uncertainties in the cross-sections strongly motivate that interactions be measured on the same target medium at the near and far sites.

There are therefore two physics needs driving the liquid argon TPC near detector: (1) to measure the flux of ν_μ , $\bar{\nu}_\mu$, ν_e and $\bar{\nu}_e$; (2) to do so using interactions with argon, since the baseline plan includes a liquid argon TPC at the far site.



It should be noted that a LAr TPC far detector can be expected to have the same track resolution and neutral-current π^0 and gamma identification capabilities as the near-detector LAr TPC. This is in contrast to the monolithic water Cherenkov detectors: the technology used to obtain fine-grained resolution in a water detector cannot be economically scaled up to the target masses required at the far detector. This is a major motivation for the development of LAr TPCs for both far and near detectors.

In the reference design, two options are considered. Option one is to relocate and recommission the MicroBooNE LAr TPC for use as a near detector [MicroBooNE]. MicroBooNE is a project and experiment to build a LAr TPC for physics and R&D purposes and has long been an integral part of the “integrated plan” for the LBNE LAr TPC [IntegratedPlan]. Option two is to build a new LAr TPC according to the “modular design” developed by the UCLA group [UCLA-TPC]. This design incorporates a “modular” approach to cryostat design, and adds the possibility of placing the TPC in a magnetic field for charge sign identification and the separation of ν_μ , $\bar{\nu}_\mu$, ν_e and $\bar{\nu}_e$ events.

4.4.2 MicroBooNE Detector Option

MicroBooNE will be a ~ 70 ton fiducial volume Liquid Argon Time Projection Chamber (LArTPC). It is its own experiment and project, currently finishing its technical design review for CD-2. Prior to the time when the option to retask it for LBNE would be exercised, MicroBooNE will be exposed to the Booster Neutrino Beam (BNB) with 6×10^{20} protons on target, as well as to an off-axis component of the NuMI beam. This data will be used to measure neutrino cross-sections on argon, address the MiniBooNE low energy excess, and demonstrate its capabilities for distinguishing between photons and electrons and good particle identification in general.

4.4.2.1 Detector Design

The figure below shows a cross section of the proposed detector (from the MicroBooNE conceptual design report [MBCDR]).

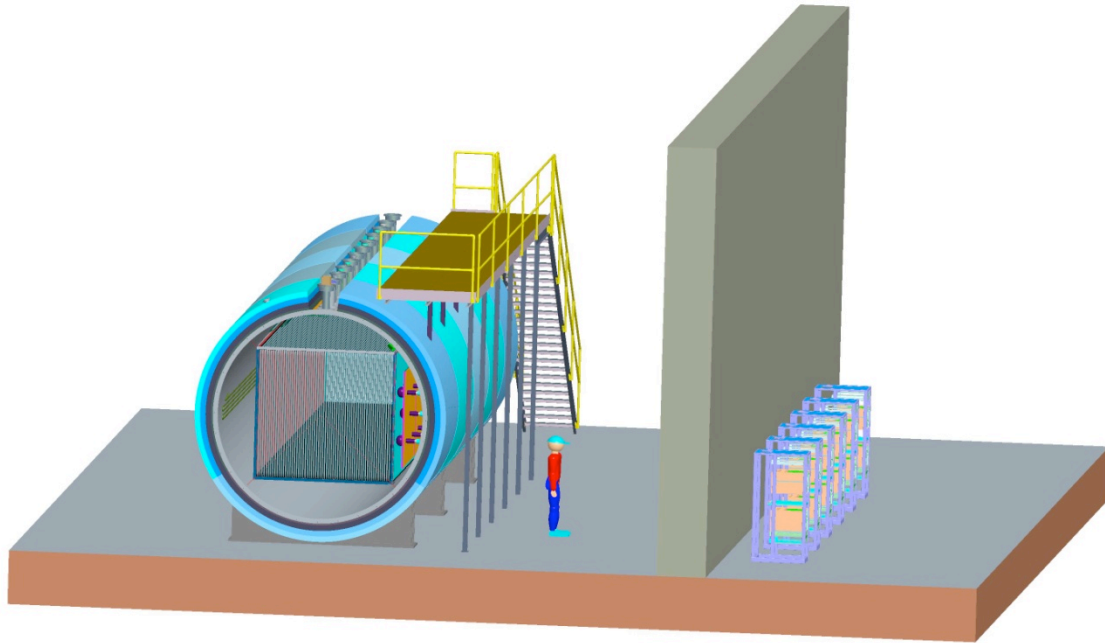


Figure 0-4: TPC inside cryostat

Cathode plane is on the left (beam left). Wire planes are on the right (beam right). PMT array is in the beam right line.

The main components of the detector are:

- The cryostat.
- Wire planes forming a high voltage box of uniform field along the ion drift direction.
- “Cold electronics”: pre-amplifiers in the cryostat, as close as possible to the readout wires.
- Photo-multiplier tubes (PMTs) to provide start times for events without a beam trigger.
- Hermetic feed-throughs for the signals, calibration lines, pre-amplifiers power, high voltage, and monitoring lines.

Attached to the detector are the following systems:

- High voltage supplies.
- Digitizing electronics.
- Cryogenic systems for the liquid argon, purification and purity monitor systems.

4.4.2.2 Reference Parameters

MicroBooNE reference parameters: The MicroBooNE detector is described in great detail in the MicroBooNE conceptual design report [MBCDR].

Detector performance goals:

- Efficiency of distinguishing electron showers from photon showers: >80%
- π^0 contamination of electron-id events: less than 6%.

- Energy Resolution: < 12% at 100 MeV (cosmic muons)
- Angular Resolution: < 5° at 100 MeV (cosmic muons)
- Spatial Resolution: < 5 mm
- Fiducial Volume: >60 ton

Physics signal (dE/dx) dynamic range and resolution: >50, sufficient to distinguish 1 MIP from 2 MIP particles traveling perpendicular to the wire direction and identify highly ionizing slow particles traveling along the wire direction.

Detector properties:

- Cryostat: inner diameter of 4 m, inner length 12 m. Outer diameter 4.67 m, outer length 13 m.
- Argon purity: < 30 ppb.
- TPC active volume: 2.3m x 2.6m x 10.4m.
- TPC field: 500 V/cm
- Drift velocity: 1.6 mm/ μ s
- Maximum drift length, cathode to anode: 2.6 m (transverse to long axis of cryostat)
- High voltage: 130 kV
- Wire spacing: 3 mm
- Wire planes: 2 induction planes (U, V) with wires running at 30°, 150° with respect to the beam direction (z-axis), and 1 collecting plane (Y).
- Total number of TPC channels: ~10k
- Sampling rate: 2 MHz (multiple samples per preamp shaper peaking time).

The following tables are taken from the MicroBooNE conceptual design report [MBCDR].

Detector Requirements		
Parameter	Value	Motivation
Energy Resolution	< 12% at 100 MeV (cosmic muons)	Equal to or better than MiniBooNE energy resolution
Angular Resolution	< 5° at 100 MeV (cosmic muons)	Equal to or better than MiniBooNE angular resolution
Efficiency of distinguishing electron showers from photon showers	>80%	Sufficient efficiency to resolve the MiniBooNE low energy excess
Spatial Resolution	< 5 mm	Sufficient resolution to resolve the MiniBooNE low energy excess
Fiducial Volume	>60 ton	Acquire a sample of 10,000 neutrino interactions with the currently achievable BNB neutrino flux.
Physics signal dynamic range	>50	1) Distinguish 1 MIP from 2 MIP particles traveling perpendicular to the wire direction 2) Measure dE/dx of highly ionizing slow particles traveling along the wire direction (~50 MIP's)

Table 0-2: LAr detector requirements

Cryogenics & Purification System Requirements		
Parameter	Value	Motivation
Argon purity	<30ppt O ₂ <1ppm N ₂	Need to identify a minimum ionizing particle at the longest drift distance.
Liquid argon receiving rate	One tank truck per day	
Cryostat LAr temperature range	<1°K	Eliminate the effect of convection currents on the electron drift
Pressure stability	<2 PSI during operation	
Purification flow	1 volume change/day	Ensure that adequate purity can be achieved after filling the cryostat
Backup control power	>24 hours	Safety – maintain the functionality of the ODH alarm and monitoring during power outage
Access to vessel interior	Head removable up to 1-2 times during experiment run	Allow for repair/replacement in case of loss of detector function. Vessel would have to be removed from the enclosure for head removal to occur
Cryostat insulation	<13 W/m ²	Eliminate the effect of convection currents on the electron drift
LAr bubble formation	None	Eliminate the effect of convection currents on the electron drift
Cryostat MAWP	30 psig/full vacuum	
Seismic load	UBC Zone 1	

Table 0-3: Cryogenics and purification system requirements

Active Detectors Requirements		
Parameter	Value	Motivation
TPC Dimensions	2.325 m vertically x 2.564 m horizontally x 10.400m in the beam direction as measured from the edges of the wire carriers.	The transverse size fits within the cryostat vessel that can be transported to Fermilab by truck. The length is determined by the fiducial volume requirement.
Wire Pitch	3mm	3mm is the minimum wire pitch possible given the electronics S/N and the expected purity and satisfies the spatial resolution detector requirement.
Wire Plane Separation	3mm	Wire plane separation should be roughly equal to the wire pitch.
Wire diameter	150 microns	Large enough to withstand the tension put on the wire.
Wire Tension	1kg	Tension is set so that there is no more than 0.5mm sag for a 5m long wire.
Wire length construction tolerance	± 0.01% or ± 0.25mm	Provide small and repeatable wire sag. For a 2.5m wire, this represents <± 5% tension variation at 1kg which corresponds to pm 0.025mm of sag
Wire composition	150 μm stainless steel wire, 2 μm copper plating with gold flash	Copper plating reduces electronics noise. Gold flash provide oxidation protection.
Number of read out	3	Redundancy is necessary to reconstruct

wire planes		tracks traveling along a wire direction in one plane
Wire orientation	1 vertical plane, 2 planes at ± 60 degrees from the vertical	Large angle tracks from low energy neutrino interactions require large angle differences between wire plane orientations.
Photo-multiplier tubes	30 8" diameter PMT's	Sufficient photocathode coverage to trigger on protons from π -p elastic scattering events down to 40 MeV.

Table 0-4: Active detector requirements

High Voltage Requirements		
Parameter	Value	Motivation
Cathode Voltage	125kV	500V/cm nominal operating drift field. Power supply capable of 150kV (or up to 600V/cm drift) .
Ripple tolerance	$<1 \times 10^{-5} V_{pp}@1mA$ load	Eliminate drift velocity variations and external noise

Table 0-5: High voltage requirements

Electronics & DAQ Requirements		
Parameter	Value	Motivation
Dynamic Range	$< 500:1$	Physics signal dynamic range * 10:1 signal/noise requirement
Noise	ENC < 660 electrons with 1 μs shaper peaking time	Distinguish 3 fC wire signal (1 MIP) from noise with high efficiency at the longest drift time (1.6 ms) with an electron lifetime of 1.6 ms.
Beam trigger readout time	4.8 ms	The TPC drift time is 1.6 ms. Samples are taken 1.6 ms before and 1.6 ms after a beam spill to reconstruct out-of-time cosmic muons
Shaper peaking time	$\sim 1 \mu s$	The average electron diffusion over a the drift distance is ~ 1.4 mm = $\sim 1 \mu s$.
ADC sampling rate	~ 2 MHz	The sampling rate should be at least 4/(shaper peaking time).
ADC resolution	~ 12 bit	Minimize the rate of ADC overflow for low momentum, highly ionizing particles
Data buffer storage	<u>Accelerator neutrino physics:</u> none <u>Supernova physics:</u> one hour of continuous data	Sufficient time to await supernova notification by SNEWS

Table 0-6: Electronics and DAQ requirements

MicroBooNE power, cooling, and other infrastructure requirements:

Power and cooling requirements:

- Electronics area: 300 kW (12 racks at 25 kW), cooled to 72 degF to 75 degF, 50% RH max, no min RH.

- Cryostat and cryogenics area(s): < 200 kW power, 60 degF min, 80 degF max, 55% RH max, no min RH.

Facilities and infrastructure: A structure within the experimental hall is required to contain the MicroBooNE detector and cryogen systems for oxygen deficiency hazard mitigation. Space for 12 racks of electronics is also required.

4.4.2.3 LAr R&D

An integrated R&D plan for a very large Liquid Argon Time Projection Chamber (LArTPC) has been prepared by the LArTPC Planning Group^{{\cite{IntegratedPlan}}}. The integrated plan includes both hardware and physics R&D for a LArTPC for the Long Baseline Neutrino Experiment (LBNE), focusing on a 20 kiloton design referred to as LAr20. This plan also includes development of the smaller LArTPC MicroBooNE, which is suitable as near detector for LBNE. The integrated plan outlines existing components, current activities, and new efforts required to fully demonstrate the LBNE LArTPC option.

The R&D absolutely required for the near detector are as follows:

- Hardware R&D
 - Argon Purity: Achieve and maintain purity in an un-evacuatable vessel.
 - Electronics: Develop cold, low-noise electronics with channel multiplexing in the LAr.
 - Active detector systems (TPC): Design TPC modules and light collection systems.
 - Cryogenics: Develop cryogenics systems for operation deep underground.
 - Underground Issues: Address issues related to siting of a detector deep underground.
- Physics R&D
 - Analysis tools: Develop tools to simulate and reconstruct neutrino interactions
 - Surface operation of a physics experiment: Test feasibility to reconstruct data in a detector exposed to cosmic ray backgrounds on the surface.
 - Physics results: Produce publishable physics results with a large experiment

In addition, cryostat development for membrane and modular style cryostats that can be scaled up to very large size for use in the far detector lab. These cryostat options are expected to be significantly cheaper than the conventional, evacuatable cryostats used for existing LAr TPCs.

All of the physics studies and hardware R&D for the LArTPC option for LBNE near detector are being pursued in the context of ArgoNeuT, MicroBooNE, and Liquid Argon Purity Demonstration (LAPD) projects. The figure below shows the present and proposed R&D activities for the entire Integrated Plan for LAr TPC development for near and far LBNE detectors.

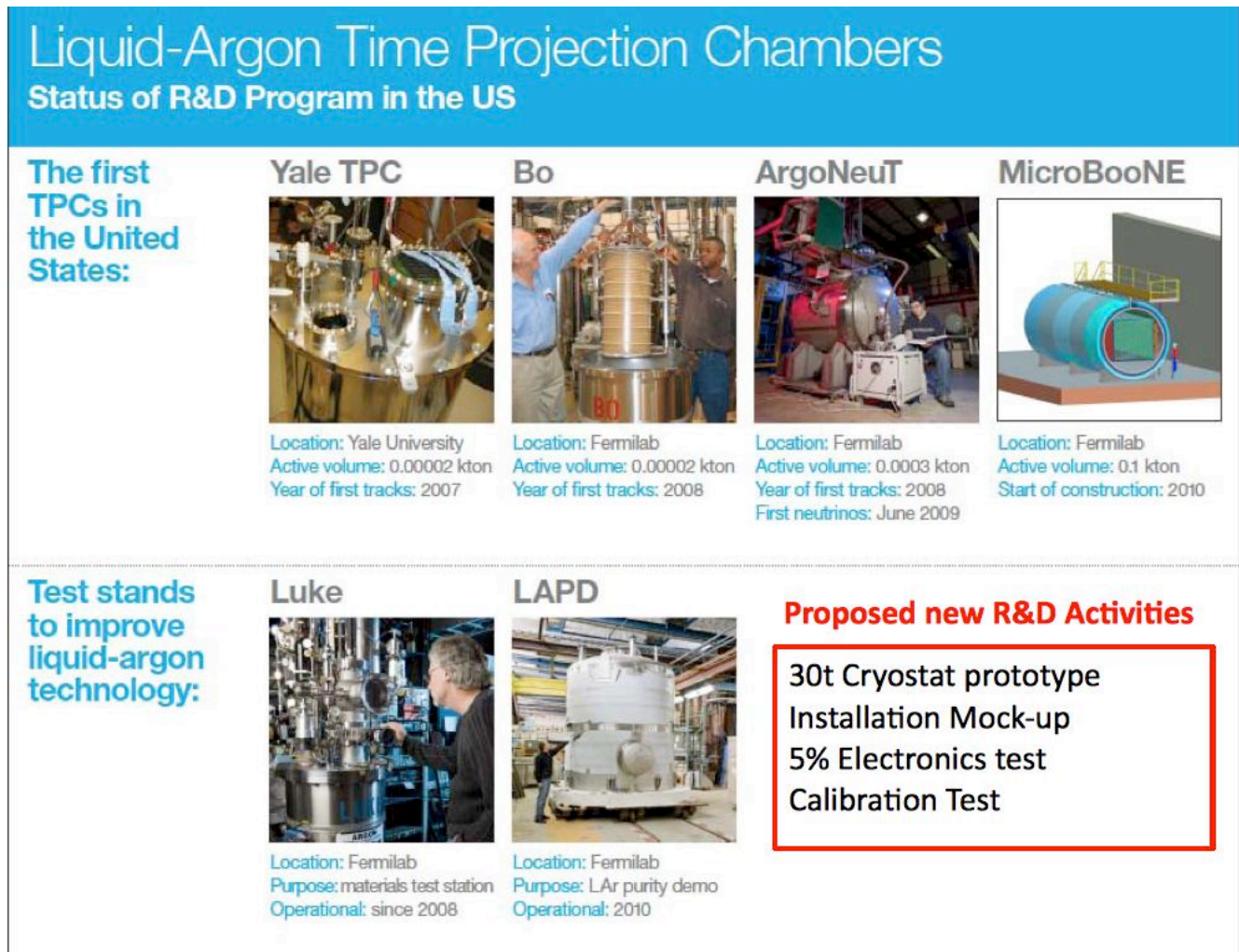


Figure 5: Status of LAr TPC R&D in the U.S.

4.4.2.4 Safety issues

The unique safety issues associated with the LAr TPCs include oxygen deficiency hazards associated with liquid argon and high voltage safety for the 130 kV TPC bias. The following requirements are copied from the MicroBooNE conceptual design report [MBCDR]:

Cryostat and cryogenics systems ES&H: A hazard analysis for the components of these subsystems will be performed, including a list of relevant Fermilab safety requirements and how they will be addressed.

The use of liquid argon makes the MicroBooNE site a potential oxygen deficiency hazard (ODH) area. The area will be analyzed and classified according to Fermilab ODH standards. Based on the results of that analysis appropriate ventilation, oxygen sensors, alarms, signs and training will be implemented. Besides the indoor spaces normally covered under the Fermilab standards, potential outdoor problems will also be studied. It will also include a discussion of secondary

containment, despite the absence of national standards requiring secondary containment for liquid argon storage.

The liquid nitrogen and argon are also extremely cold and can cause frostbite if they come in contact with skin. Individuals making connections between the delivery trucks and the system must wear protective equipment including gloves, aprons and face shields. Individuals working with the plumbing system must do so as well. There will be training provided and people will have to be qualified for tasks involving either ODH or cryogenic hazards as provided in the FESHM.

Fermilab environmental safety and health standards will be followed in the design and implementation of the cryogenic system.

Electronics:

Personnel involved in this work must complete all necessary training (e.g. cryogen safety, electrical safety) in compliance with federal and state regulations and with DOE orders.

Power and DAQ rack protection requirements will be evaluated and the proper protection will be installed to assure the safe operation.

Installation and commissioning:

The cryostat is 3.8m (12.5') in diameter and 13m (44') in length. The cryostat is not considered a confined space during assembly since there is ample space for egress (2.5m vertical x 2.5m horizontal). No hazardous materials, flammable materials or oxygen displacing gases will be used inside the cryostat during assembly. No welding will be done inside the cryostat. Exterior welding of the cryostat chimneys will be done in accordance with ASME Section VIII or ASME/ANSI B31.3.

The maximum distance personnel must travel to exit the cryostat and clean room is 19m (62'). NFPA 101.13.2.6.2 allows a maximum total length of travel of 250' from any point in a sprinkler protected building to an exit. The maximum distance personnel must travel in Lab 6 to an emergency exit with the detector cryostat in place is comfortably below 250'.

The TPC will be tested for voltage breakdown several times during assembly. There is a risk of electrical shock if an end cap is not attached. This risk will be mitigated by the use of a LOTO procedure for operation of the high voltage supplies.

References

- [**Integrated Plan**] LArTPC Planning Group, B. Baller and B. Fleming, Editors. "Integrated Plan for LArTPC Neutrino Detectors in the U.S.," LBNE Project-doc-113-v1, November 2009.
- [**MBCDR**] MicroBooNE collaboration, B. Baller, editor, B. Fleming, spokesperson. "MicroBooNE Conceptual Design Report," MicroBooNE Document 340-v10, February 2010.

4.4.3 UCLA Detector Option

The liquid Argon near detector has been proposed as one of the four potential detectors to support the Long Baseline Neutrino Experiment and to be sited in the Near Detector Experimental

Hall approximately 400 ft under the surface and approximately 700 m from the pion production target and the focusing lenses.

The magnetization of the LAr TPC adds the charge separation capability, particularly for the electrons and the positrons for the detection of the GeV electron neutrinos and anti-neutrinos. For beam flux measurement to the precision of 3% level or below, the neutrino fluxes need to be measured also to this similar precision. Below we show CAD concepts on how to achieve a magnetized LAr TPC of about 20 tons in order to distinguish neutrino events from antineutrino events. A small magnetized TPC was built and tested by A. Rubia et al. in 2005. Images in Fig. 1 show good quality tracks under 0.55 T field.

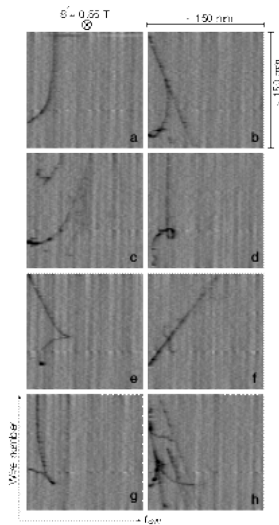


Figure 1. Recorded events in a small 15.0 cm \times 15.0 cm magnetized TPC by A. Rubia et al. [1]. The bending curvatures have radii of 5 cm to 10 cm in the field of 0.55 T, indicating momenta of 15 MeV/c.

We made a crude estimate using the CC event rate plot by M. Bishai on the required detector size to get 1% statistical precision. The graph in Fig. 2 shows that there are about $5 \times 10^5 \nu_e$ CC events per GeV. Then, to get 10^4 events per GeV per year requires a detector mass of 30 ton assuming a beam power on target of 700 kW. We begin with a small mass detector of 20 ton in our design and show the possible extension of the detector to a larger mass.

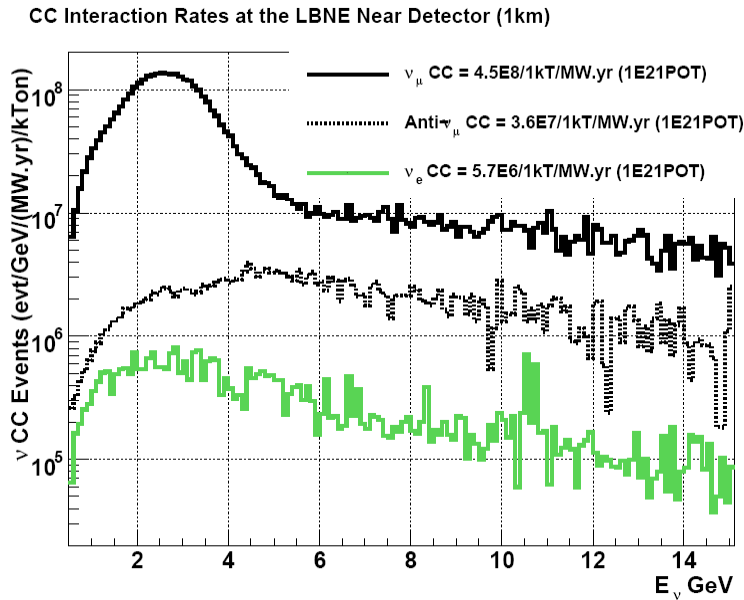


Figure 2. Charge current rates by M. Bishai [1] at the near detector at 1 km from target.

4.4.3.1 Detector Design

Various LAr TPC cryostat vessels have been designed by UCLA members in connection to the large scale proton decay and neutrino beam far detector. Over the past decade, the design work converged onto scalable structures that are built on cubic cells or hexagonal parallelepiped cells. As the magnetization was considered for the LAr vessel, it was realized that the cost challenge of magnetizing a large volume of several cubic meters, either in the form of electric power usage of $\sim 1 - 2$ MW or the cost of superconducting wires. A number of ways were investigated over how to wind high temperature superconducting (HTS) wires around the detector vessel. The known challenge is how to find an economical way of thermally insulating the HTS wires in order to maintain them at the required low temperature either at or below the liquid N_2 temperature. For the LAr detector, the solution appears to be to keep the coil within the vacuum volume, outside of the LAr vessel.

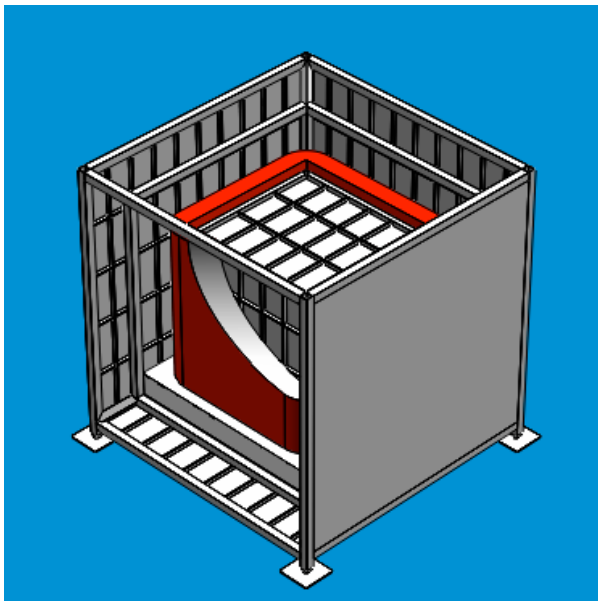
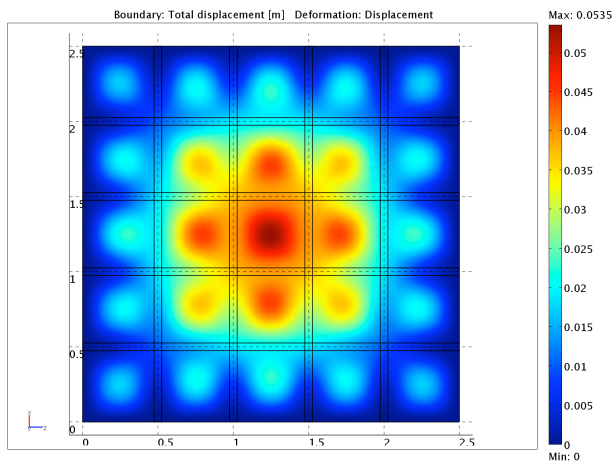


Figure 3. The LAr volume is $2.5 \text{ m} \times 2.5 \text{ m} \times 2.5 \text{ m}$ dimensions with a rectangular coil of $3.0 \text{ m} \times 3.0 \text{ m}$ on the sides and 3.0 m high. The LAr vessel and the coil sit inside the center of the $5.0 \text{ m} \times 5.0 \text{ m} \times 5.0 \text{ m}$ volume. The outer cubic volume is formed by the steel frames of $6.0 \text{ in} \times 6.0 \text{ in}$ square hollow beams and panels of 1.0 in in thicknesses with supporting bars welded on.

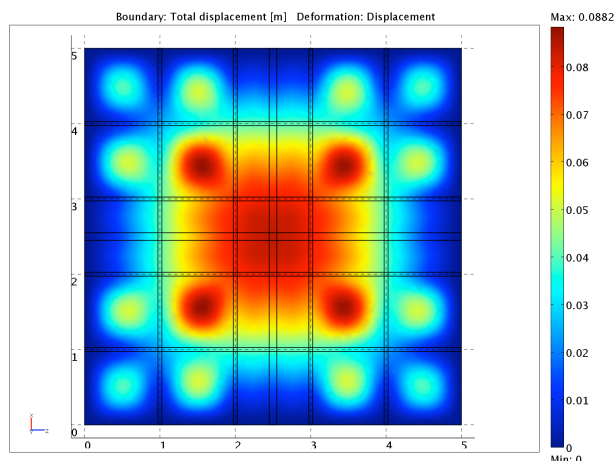
The drawing in the above Fig. 3 shows a cutaway view of a rectangular coil containing the cubic structure of $2.5 \text{ m} \times 2.5 \text{ m} \times 2.5 \text{ m}$ volume. The central volume can hold up to 22 tons of LAr. The coil and the LAr vessel sits on an insulation layer thermally isolated from and mechanically supported by the $4.0 \text{ m} \times 4.0 \text{ m} \times 4.0 \text{ m}$ cubic structure which is joined to the external $5.0 \text{ m} \times 5.0 \text{ m} \times 5.0 \text{ m}$ structure at the eight corners. This concept is the result of merging the scalable cubic vacuum concept by F. Sergiampetri and the simpler structural concept of a tank sitting within a tank of the non-evacuatable far detector version. By having the LAr vessel not connected mechanically, there is less concern of shrinkage of the inner vessel relative to the external vessel sitting at room temperature. The coil structure is also not connected mechanically to the inner LAr vessel or to the outer vessel, hence it has a slack of shrinkage when cooling down to 20 K. The scheme allows for sufficient space not only for the coil with the Helium cryogenic tubing and the insulation to sit in but also for the field return soft iron yoke structure, not shown. The windows of the outer structure can be padded with soft iron to function as the field-return yoke. However, the field uniformity within the coil volume can only be achieved with a large iron structure with symmetry and sufficient thickness.

The window planes at this time are formed by steel sheets and steel bars crisscrossing horizontally and vertically. Below in Fig. 4, deformation of the window under the pressure of 10 atm was studied by finite element calculation for both the $2.5 \text{ m} \times 2.5 \text{ m}$ and the $5.0 \text{ m} \times 5.0 \text{ m}$. It was a surprise to find that steel bars of at least 6.0 in height were necessary to keep the window plane from bulging out severely. For the $5.0 \text{ m} \times 5.0 \text{ m}$ window, 12.0 in height bars were used and the maximum deformation is about 8 cm. These simple structures with rectangular steel bars of corresponding heights appear to be capable of holding the window under excessive pressure application of 10 atm. In the future, when more information becomes available on the engineering safety requirement, the window material specification can be changed, and also the support structural design changed to more economical designs studied by UCLA members for the evacuatable version of the far detector.



a)

Figure 4a. $2.5 \text{ m} \times 2.5 \text{ m}$ window with 0.5 in thick steel sheet and 2.0 in \times 6.0 in steel solid bars as backing ridges. Applied outward pressure is 10 atm. The maximum deformation is 5 cm.



b)

Figure 4b. 5 m × 5 m window with 1.0 thick steel sheet, two 4.0 in × 12.0 in and eight 2.0 in × 12.0 in steel solid bars as backing ridges. Applied outward pressure is 10 atm. The maximum deformation is 8 cm.

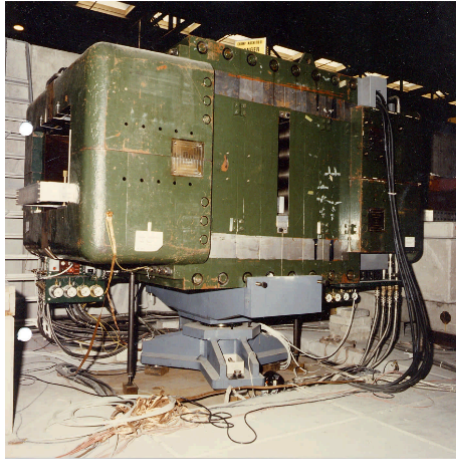
The parallelepiped cryostat vessel as mentioned above is the result of designs by UCLA members who have considered solutions for scalable TPC structural units. In the future, costing will be investigated for using cylindrical shape vessel. The advantage of the cubic shape vessel is that it allows for prototyping work for a large scale detector in the future. In addition, it is easily extensible in 1-D for a longer length LAr vessel. This scheme is also not too different from the concept by F. Sergiampetri that is also scalable in 3-D with proper design of coupling between the inner LAr vessel and the outer vacuum vessel. For the large scale vessel, the thermal contraction of 304 SS material can be as much as 8 cm over the 40 m dimension. There is serious displacement of the inner vessel relative to the outer vessel for the 304 SS material. However, there are other steel alloys such as Pernifer36 by Thyssenkrupp-VDM which advertises to have supplied 70 metric tons to the ICARUS detector. The Pernifer36 has extremely low thermal contraction at only 10^{-6} for liquid nitrogen temperatures. Chemical compositions in Table 1 shows that Pernifer36 has much more Ni than the 304SS and the 316SS and almost no Chromium.

	Cr	Ni	C	Mn	Cu	Mo	Si	S	P	
304 (MM)	19-20	9-12	0-0.09	0-2	0-1	0-1	0-1	0-	0-0.2	
316 (MM)	16-19	10-14	0-0.09	0-2	0-	0-3	0-1	0.03	0-	N 0-
Pernifer36	0.25	35.0-37.0	0.15	0.60	0.75		0.40	0.025	0.025	Co 0.1
										0.50

Table 1. Chemical Composition of Steel Types

4.4.3.2 Magnets

Magnetizing a large volume to a field of 1T has been accomplished previously in large dipole magnets such as the UA-1 magnet. In the process of considering ways of magnetizing the LAr volume, we have listed below one dipole magnet at CERN as potentially available, following on the prior work by F. Sergiampetri and others in a proposal back in 2002 to magnetize a small LAr volume.



Magnetized volume dimensions:	Gap.....	120 cm
	Aperture...	80 cm
	Length....	200 cm
Field:.....		1.08 T
Power:.....		1000 A
		1200 kW
Weight:.....		100 tons
Outline Length.....		3.8 m
Width.....		2.1 m
Height.....		2.4 m

Figure 5: The CERN MNP 101 magnet and its main parameters.

The volume available within the magnet appears to be small after we had determined the required detector mass to be 30 tons. Below in Fig. 6 is a drawing of a cryostat vessel inside a cutaway view of the MNP 101 magnet. The external dimensions of $0.7\text{ m} \times 0.7\text{ m} \times 3.2\text{ m}$ for the cryostat vessel give only about 1.7 ton LAr mass.

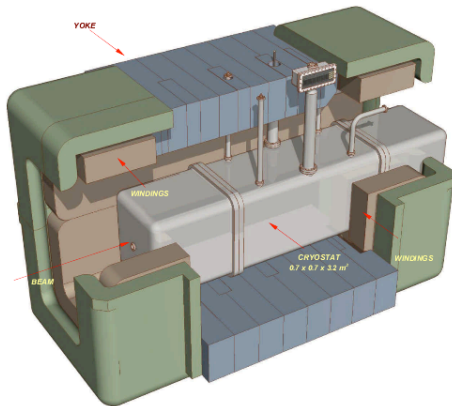


Figure 9: The proposed LArTPC cryostat installed inside the MNP101 magnet.

Figure 6. LAr cryostat vessel drawn for the CERN MNP 101 magnet.

However, in the course of looking into the use of high temperature superconducting (HTS) wires, it appears possible to build a solenoid magnet confined to a compact volume as shown in Fig. 3. The HTS wire technology has matured to the point that the 2nd generation wires consisting of tapes of $3.4\text{ mm} \times 0.4\text{ mm}$ cross section are available readily from commercial vendors.

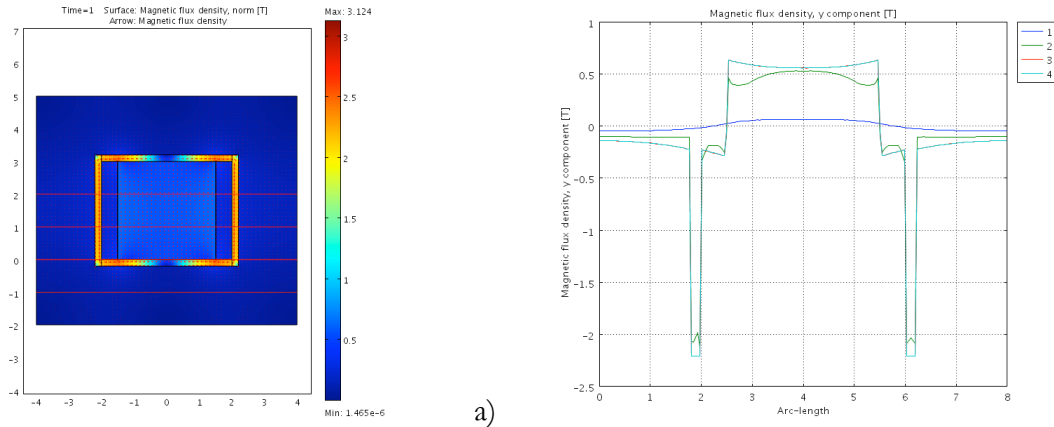


Figure 7. Finite element 2-D calculation for magnetic flux of dipoles of 3.0 m width and 3.0 m height with 7.35 kA/cm current in the coil and with return iron yoke of 20.0 cm. The B field of the dipole varies by nearly 12% from 0.57 T at the center to the sides. The abscissa scale corresponds to -4.0 m to $+4.0$ m. The various field curves correspond to the cross section lines indicated in the pictorial graphs with no. 1 at the most bottom.

For the magnetization, a 0.5 T field is set as the goal of the coil investigation. The field uniformity requirement is not well known at this time until event simulation studies have been done with GEANT4. However, it is reasonable to assume that a known field map with known rolling variation is sufficient for precise event kinematics reconstruction. In Fig. 7, plots are shown for a finite element field calculation of a 2-D dipole with 3.0 m width \times 3.0 m height. Surrounding on top, bottom and the two sides are soft iron walls for field return yoke. On the left side of the figure 4a and 4c are for 20.0 cm wall and on the right side 50.0 cm wall. A larger iron mass minimizes the field variation and also gives a nearly 40% higher field at 0.8 T vs. at 0.6 T. Future calculation will incorporate the corners in 3-D models.

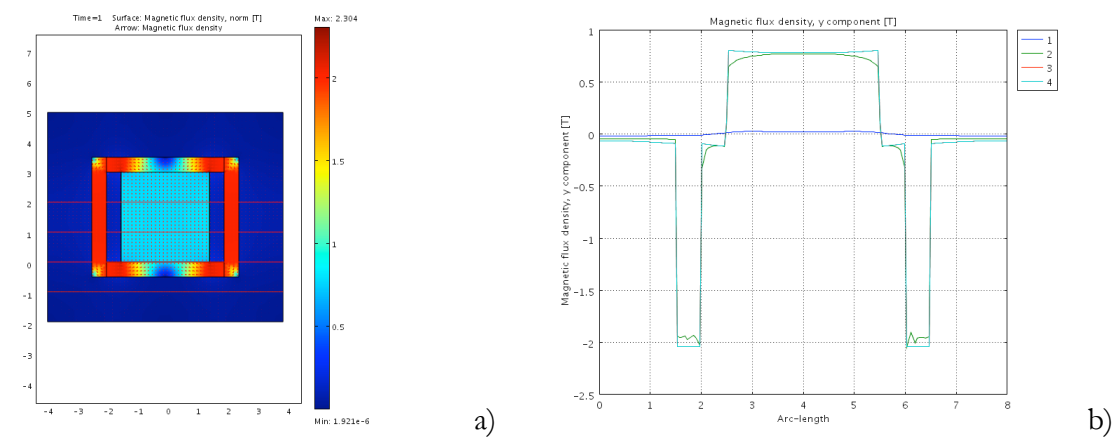


Figure 8. Finite element 2-D calculation for magnetic flux of dipoles of 3.0 m width and 3.0 m height with 7.35 kA/cm current in the coil and with a return iron yoke of 50.0 cm. The B field of the dipole, 0.78 T, varies from the center to the sides by only 3.5%.

The current linear density is 7.35 kA/cm and is based on the nominal current throughput of 100 A at liquid Nitrogen temperature.

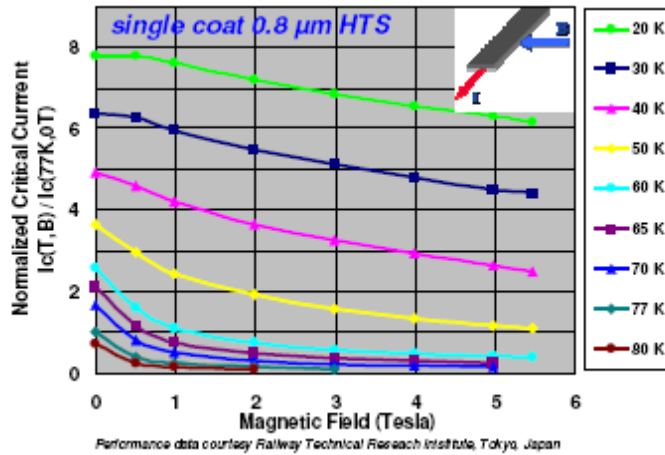


Figure 9. Wire Performance with Magnetic Field Parallel to Tape Surface. Operating the HTS wires at ~20 K increases the critical current by 7.5 times at 1 Tesla parallel field. Courtesy of American Superconductors.

The coil requires Helium gas cooling to achieve the 30 K temperature or lower and is also to be isolated from the LAr inner vessel which can be only a little below the 87 K LAr boiling point. The coil can be constructed by winding around a rectangular structure of 3 m × 3 m × 3m dimensions with round corners. It is critical to choose proper structural material to match the thermal shrinkage of the HTS tape, which has stainless steel or brass as the stabilizer. For Be-Cu alloy, the integral thermal contraction is around 0.003 for a temperature decrease from 293 K to 20K. The 3 m dimensions coil structure will shrink by 9 mm. The HTS tape with the brass stabilizer will better match the Cu coils for the He cooling. This can be studied in the future. During operation the coil will experience a large outward pressure of 106 psi or 75 tons/m². The required stabilizer holding the coil back against the outward force needs to be investigated. The goal is to allow only the minimal amount of mass at 20 K. The field return iron yoke which can be as massive as 800 tons should be external to the thermal insulation of the coil. There will be questions over whether to allow a large amount of iron upstream and downstream of the LAr vessel and how best to design the iron yoke so as to not interfere with particle tracking measurement. At the same time, it appears possible to use the field return yoke, which is strongly magnetized within part of the muon rafter.

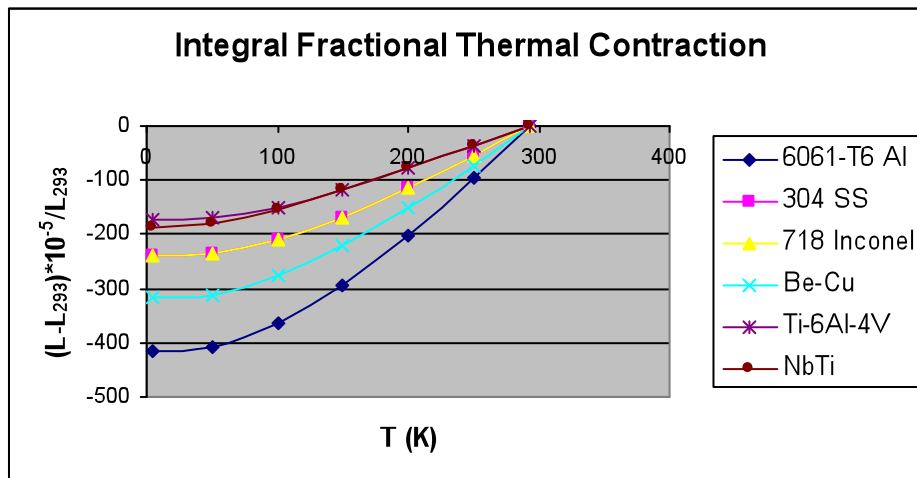


Figure 10. Cryogenic data for various materials from NIST.

The magnet system still needs to be studied in detail in the future. As mentioned already, there will be a strong outward pressure due to field current interaction. In addition, there will be a strong force between the iron yoke top and bottom with the coil. Structural support for both the coil and the yoke need to be considered in detail, along with the insulation for the coil to attain the 30 K goal. Further, there is no study done yet on quench protection. There is 11 MJ of energy stored within the coil volume. In case of a sudden temperature rise above the critical temperature, the stored energy can be dissipated via a Cu coil wound together with the He cooling coil at a rate of 36 kW over 5 minutes. If a simple quench protection system is built, it will require about 10 tons of Cu.

4.4.3.3 Power Requirement

The detector system has been designed to have very low heat leakage. Hence, a cryocooler of a few hundred watt is sufficient to balance the heat leakage into the system. The LAr pumping system is also minimal for this detector volume. There is only 125 m³ of volume in the vessel. If the pumping rate is 10 l/sec, then the entire volume can be recirculated in 3.5 hrs. The overall power requirement will be at most 10 kW to operate all of the power supplies for the detector system.

4.4.3.4 Detector Installation

The detector is to be installed in the experimental hall nearly 400' underground. The shaft for bringing material down is not large enough for the 5 m × 5 m × 5 m outer structure. Details will be given in the future. As much as possible, structures will be welded above ground.

The heaviest component in the LAr near detector is the iron yoke of 800 tons. However, as this component is only for directing the flux lines, it can be assembled into the yoke structure from smaller individual pieces. Among the remaining components, the large outer windows can be as heavy as 6 tons. Lifting the large windows and aligning them for welding onto the structure can be challenging.

The detector system is to have a secondary storage with a large volume. It is to be used for transferring the liquid Ar in case of large thermal leakage into the detector vessel or with long down time of the cooling system, whether it is for a planned shutdown or failure of the vacuum or the cooling system. It is best to locate the secondary storage away from emergency exits. A hole below the hall level can be dug for the storage vessel.

In case of an ODH hazard, personnel can climb up to elevated catwalks for escape to refuge area. Safety requirements are to be designed and implemented by the Fermilab safety personnel in the future. In general, there needs to be good continuous air flow in the experimental hall.

4.4.3.5 R&D

After one iteration of the conceptual study, a 22 ton magnetized LAr detector appears to be possible to build.

The following are the major components of the detector system:

- Cryostat vessel
- HTS magnet with Helium gas cooling and the internal field return iron yoke
- LAr recirculation pump and purification system
- TPC structure
- Photosensor (SiPM) system
- Electronics and DAQ

The first two define the feasibility of the detector system. The two components will be continued to be studied in more detail in the future with more details and with more information from material vendors for accurate modeling and costing.

Very little work has been done on the remaining four items, although this near detector project can benefit from the experience of the ICARUS project and the LBNE far detector studies.

4.4.3.6 Summary

A conceptual design of a LAr magnetized near detector system of 22 tons has been carried out. The cryostat vessel is not as detailed as previously done in connection to the far detector unit cell of 125 ton. There will be at least another iteration of the cryostat design in the future. The magnet coil of HTS wire for 0.5 T field has been investigated. The current design of the cryostat vessel, while not exactly the same conceptually as the far detector unit cell, is extensible in 1-D without much modification.

References

[Integrated Plan] LArTPC Planning Group, B. Baller and B. Fleming, Editors. “Integrated Plan for LArTPC Neutrino Detectors in the U.S.,” LBNE Project-doc-113-v1, November 2009.

[MBCDR] MicroBooNE collaboration, B. Baller, editor, B. Fleming, spokesperson. “MicroBooNE Conceptual Design Report,” MicroBooNE Document 340-v10, February 2010.